Mineralogy and geochemistry of Asian dust: Dependence on migration path, fractionation, and reactions with polluted air

Gi Young Jeong*

Department of Earth and Environmental Sciences, Andong National University, Andong 36729, Republic of Korea

*Correspondence to: Gi Young Jeong (jearth@anu.ac.kr)

Abstract. Mineralogical and geochemical data are essential for estimating the effects of long-range transport of Asian dust on the atmosphere, biosphere, cryosphere, and pedosphere. However, consistent long-term data sets of dust samples are rare. This study analyzed 25 samples collected during 14 Asian dust events occurring between 2005 and 2018 on the Korean Peninsula, and compares them to 34 soil samples (< 20 μm) obtained from the Mongolian Gobi Desert, which is a major source of Asian dust. The mineralogical and geochemical characteristics of Asian dust were consistent with those of fine source soils in general. In dust, clay minerals were most abundant, followed by quartz, plagioclase, K-feldspar, calcite, and gypsum. The trace element contents were influenced by mixing of dust with polluted air and fractionation of rare earth elements. Time-series analyses of the geochemical data of dust, combined with satellite remote sensing images, showed a significant increase of Ca content in the dust crossing the Chinese Loess Plateau and the sandy deserts of northern China. Calcareous sediments in the sandy deserts and pedogenic calcite-rich loess are probable sources of additional Ca. Dust-laden air migrating toward Korea mixes with polluted air over East Asia. Gypsum, a minor mineral in source soils, was formed by the reaction between calcite and pollutants. This study describes not only the representative properties of Asian dust, but also their variation according to the migration path, fractionation, and atmospheric reactions.

1 Introduction

Mineral dust blown from arid lands is transported to remote atmospheric, terrestrial, cryogenic, and marine environments, contributing to the circulation of earth materials (Martin and Fitzwater, 1988; Dentener et al., 1996; Biscaye et al., 1997; Jickells et al., 2005; Mahowald and Kiehl, 2003; Zdanowicz et al., 2007; Formenti et al., 2011; Jeong et al., 2013; Jeong et al., 2014; Serno et al., 2014). Asia is one of the major sources of mineral dust that are the subject of ongoing interdisciplinary research. The mineral grains of dust interact with atmospheric gases and pollutants (Dentener et al., 1996; Krueger et al., 2004; Laskin et al., 2005; Matsuki et al., 2005), which affects the bioavailability of inorganic micronutrients in remote ecosystems (Meskhidze et al., 2005; Takahashi et al., 2011). The interaction of dust particles with solar and Earth radiation influences the regional energy balance (Forster et al., 2007). The long-term deposition of dust particles on the Loess Plateau, the North Pacific Ocean, and Arctic ice sheets provides a record of paleoclimatic changes (Liu et al., 1988; An et al., 1991; Porter, 2001; Pettke et al., 2000; Bory et al., 2002; Hyeong et al., 2005; Jeong et al., 2008, 2011, 2013). Asian dust transported over long distances is an important constituent of some soils in Korea and Japan (Bautista-Tulin and Inoue, 1997; Jo et al., 2019). Iron-bearing dust transported to remote oceans has

received much attention for its possible role in phytoplankton bloom and carbon dioxide levels (Jickells et al., 2005; Johnson and Meskhidze, 2013). Mineralogical and geochemical analysis of dust extracted from pelagic sediments of the North Pacific provided a basis for determining sediment provenance and paleoenvironmental changes (Olivarez et al., 1991; Nakai et al., 1993; Leinen et al., 1994; Rea, 1994; Rea et al., 1998; Pettke et al., 2000; Hyeong et al., 2005; Serno et al., 2014).

Mineralogical and geochemical properties of bulk samples provide a basis for interdisciplinary research on long-range transported Asian dust. The earth system models involving Asian dust could be improved by adopting reliable data on dust properties. However, the bulk properties of Asian dust are poorly known due to application of widely varying analytical procedures and sample weights that are typically very low and thus usually insufficient for analysis (Leinen et al., 1994; Kanayama et al., 2002; Shi et al., 2005; Zdanowicz et al., 2007; Jeong, 2008; Jeong et al., 2014). Furthermore, analyses of scattered sample sets of limited number are difficult to detect the long-term variation of dust properties. Thus, long-term data sets obtained using consistent analytical methods could provide not only general mineralogical and geochemical properties of Asian dust for earth system modeling, but also insights into the change of dust source, migration path, and chemical interactions. However, no such data have been reported to date. Mineralogical and geochemical data for Asian dust should be compared to equivalent data for the fine silt fraction in the source soils for investigating any fractionation and reaction during the long-range transport. The currently available mineralogical and geochemical data for source soils (Biscaye et al., 1997; Honda et al., 2004; Chen et al., 2007; Jeong, 2008; Maher et al., 2009; Ferrat et al., 2011, McGee et al., 2016) are insufficient; mineralogical data are particularly rare.

The purpose of this study is to determine the mineralogical and geochemical properties of bulk dust samples collected over 14 years and compare them to equivalent data for source soils. Variations of the mineralogical and geochemical characteristics are discussed in relation to migration path, fractionation, and the interaction of Asian dust with atmospheric pollutants.

2 Samples

2.1 Asian dust

2.1.1 Outbreak and migration of dust storms

The outbreak and migration of dust storms crossing Korean Peninsula were investigated for 14 Asian dust events using an aerosol index derived from data obtained by the Communication, Ocean, and

Meteorological Satellite (COMS), which was launched on 27 June 2010 (National Meteorological Satellite Center, 2019). Pre-2011 dust events were tracked using the Infrared Difference Dust Index derived from data obtained by the Multi-functional Transport Satellite-1R (MTSAT-1R) (National Meteorological Satellite Center, 2019). Data for 2005 dust events were not available. Four satellite images were selected from the serial image set (1~0.5 h intervals) of each dust event to show 1) the extent of the dust outbreak (i.e., the point where the dust storm reached its maximum size without notable migration), 2) dust migration toward the Korean Peninsula, 3) dust crossing the Korean Peninsula, and 4) dust leaving Korean Peninsula toward the North Pacific Ocean. The dust region identified from the dust index images was drawn on a geographic map including the Gobi Desert, sandy deserts of northern China, and Loess Plateau. The outbreak and migration of each dust storm identified from satellite images are provided in Supplementary Fig. S1. Fig. 1 is a summary of the outbreak and migration of all the dust storms. The outbreak of dust storms was concentrated in the Gobi Desert and sandy deserts encompassing southern Mongolia and northern China (Fig. 1a). The 2013 dust storm occurred in the Loess Plateau as well as deserts (Supplementary Fig. S1). The dust storm migrated eastward and southeastward (Fig. 1b). The migration routes of dust storms toward the Korean Peninsula can be divided into two groups: 1) those crossing the Loess Plateau and 2) those making a detour around the north of Loess Plateau. Six dust storms (D3–6, D7, D10–11, D12, D19–20, and D21–23 in Table 1) crossed loess plateau (Supplementary Fig. S1). Dust-laden air parcels passing the Korean Peninsula are dispersed and diluted progressively, and migrate eastward and northeastward toward the North Pacific Ocean (Figs. 1c–d).

2.1.2 Size distribution

Volume size distribution was measured with an optical particle counter (OPC, GRIMM Aerosol Technik Model 180) at dust monitoring station nearest to sampling site operated by Korea Meteorological Administration (2019). The OPC reported particle numbers over 31 size bins from 0.25 to 32< μm. Sample air was directly fed into the measuring cell at a volume flow of 1.2 liter/minute by passing through a TSP head. OPC data for pre-2010 dust events were not available. The volume size distributions revealed that the modal volume diameters of most dusts were between 2–5 μm with an average size of 4.6 μm (Fig. 2). The volume size distribution of very coarse dust for a 2012 dust event showed an almost monotonic increase toward larger sizes (Jeong et al., 2014). Zdanowicz et al. (2007) reported a modal volume diameter of 4 μm of Asian dust transported long distances in April 2001, (to the Yukon Territory, Canada); larger particles (> 10 μm) were also found, indicating rapid trans-Pacific transport in the mid-troposphere. Serno et al. (2014) reported a particle-size mode of around 4 μm for

eolian dust separated from deep-sea sediments of the subarctic North Pacific Ocean.

2.1.3 Sampling

Twenty-five samples of Asian dust were cut from 2005 to 2018 at three sites, including Deokjeok Island off the western coast of Korea, Andong National University in Andong, and the Korea Institute of Science and Technology in Seoul (Fig. 3 and Table 1). Dust particles were collected on Whatman No. 1441–866 cellulose filter paper; via Tisch Environmental and Thermo Scientific high-volume total suspended particulate (TSP) samplers installed on building roofs. Jeong (2008) reported on the mineralogical properties of eight dust samples collected during 3-year period (2003–2005). However, his samples were collected using PM_{10} samplers; these exclude coarse particles, which are an important component of some dust events (Jeong et al., 2014). For some events, dust samples were collected at three sites, whereas the samples for other events were collected at one or two sites, depending on the dust migration path. For short events (a few hours in duration) one sample was collected, while 2~4 time-series of samples were collected at one site during longer events (several days in duration). The mineralogical properties of three TSP samples reported by Jeong et al. (2014) were re-analyzed to ensure consistency in the analytical procedures.

2.2 Source soils

The 34 surface soils were sampled in the Mongolian Gobi Desert along a track of 1,700 km long in the region ca. E100º~109º and N42º~46º(Fig. 3 and Table 1). The surface soils of Gobi Desert are not dominated by the sands typical of sandy desert, instead being characterized by a mixture of pebbles, sand, silt, and clays, although sand dunes are locally distributed. The bare ground, comprising loose silty soils with sparse vegetation and the dry beds of ephemeral lakes, promotes the outbreak of dust plumes under strong winds caused by a cold front system, or by a strong pressure gradient at the surface (Chun et al., 2001). About 1 kg of soil samples were taken from the surface after coarse pebbles were removed. All the soil samples were in the naturally dry state at the sampling time.

3 Analytical Methods

3.1 Sample preparation

The cellulose filter papers were shredded into several pieces, each approximately 3×5 cm^2 in size, and

subjected to ultrasonic agitation, in methanol in a 250 mL glass beaker, to detach dust particles from the filter. Cellulose fibers were removed from the dust suspension by passing through a 270 mesh sieve. The dust suspension was dried on a clean glass plate, and then collected with a razor blade for X-ray diffraction (XRD) and chemical analysis. Soil samples were passed through clean 2 mm sieve to remove pebbles. The 2-mm fraction soils was sieved under dry conditions through a disposable nylon 20-μm sieve, using a Retsch sieve shaker. 2 g of the soil separate (< 20 μm) was mixed with ethanol and ground using a McCrone micronizing mill for 7 min with zirconia grinding elements. The dust samples were not ground for XRD analyses to avoid mass loss during the milling, because the dust samples were very small (< 300 mg) and already sufficiently fine for XRD analyses. However, one sample collected during the coarse dust event was ground in an agate mortar.

3.2 XRD analyses

Since the weight of the dust samples was insufficient for conventional XRD analysis, XRD data were collected over a long time period (~12 h). Dust powders were loaded onto a small cavity (~ 7 × 20 mm^2) in a silicon plate for XRD analysis by side packing to minimize preferred orientation of mineral grains (Moore and Reynolds, 1997). The XRD analyses were performed using a Rigaku Ultima IV diffractometer at the Center for Scientific Instruments, Andong National University. The analytical conditions were as follows: counting time, 20 s per 0.03º step; 2θ, 3–65º; divergent slit, 2/3º; scatter slit, 2/3º; receiving slit, 0.15 mm; and Cu Kα radiation, 40 kV/30mA. The counting time was doubled for the samples of very low weight. Given their higher weight, the soil powders were loaded on the 20 × 20 mm^2 cavity by side packing, and analyzed at a scan speed of 0.25º per min. Mineral identification based on the XRD patterns was carried out with DIFFRAC.EVA software (Bruker AXS).

Twelve minerals (quartz, plagioclase, K-feldspar, illite, illite-smectite mixed layers, chlorite, kaolinite, amphibole, calcite, dolomite, gypsum, and halite) were quantified using SIROQUANT software (Sietronics Ltd.) with application of the Rietveld refinement technique. Background subtraction was performed carefully because samples enriched with poorly-crystalline clay minerals have high and unresolvable broad diffraction bands, particularly in the range of 20–40º 2θ. The low angle region (3–10º) was excluded from the refinement. After initial refinement, the cell parameters of chlorite, K-feldspar, albite, and calcite were refined to achieve the best fit between the observed and calculated XRD patterns. Although smectite is present as a minor clay mineral in source soils and dust (Jeong et al., 2008; Park and Jeong, 2016), it was excluded from refinement because the XRD patterns of randomly oriented bulk samples are not adequate for distinguishing small amounts of smectite from illite-smectite mixed-layer clay minerals. The refinement often showed that low crystalline illite is

difficult to be reliably distinguished from illite-smectite mixed-layer minerals in dust. This was confirmed by transmission electron microscopy analyis of clay minerals (Jeong and Nousiainen, 2014; Jeong and Achterberg, 2014) and single-particle analysis using scanning electron microcopy (SEM) (Jeong et al., 2016). Thus, in this study, the illite-smectite mixed-layer minerals, illite, and smectite contents are summed and defined as illite-smectite series clay minerals (ISCMs), as in previous works (Jeong et al., 2016). Five dust samples collected in the last five years were independently quantified by single-particle analysis using SEM combined with energy dispersive X-ray spectroscopy (EDS) analysis, following the method described in the supplement of Jeong et al. (2016).

3.3 Geochemical analyses

The major and trace element contents of the soil separates were determined in Activation Laboratories (Ontario, Canada). Dust and soil samples were mixed with a flux of lithium metaborate and lithium tetraborate, and fused in a furnace. The melt was dissolved in a solution of 5% nitric acid. The solutions were run on a Varian Vista 735 inductively coupled plasma (ICP) emission spectrometer for major elements (Si, Al, Fe, Mg, Ti, Mn, Ca, Na, K, and P) and several trace elements (Ba, Sc, Sr, V, Y, and Zr). The solutions also were run on a Perkin Elmer Sciex ELAN 9000 ICP mass spectrometer for the other trace elements. For the analysis of selected trace elements (Cu, Ni, Pb, S, and Zn), samples were digested to solutions with hydrofluoric, nitric, perchloric, and hydrochloric acids, and analyzed using a Varian Vista ICP emission spectrometer. Analytical quality was controlled by using USGS and CANMET certified reference materials for calibrations, internal standards, and duplicate analyses. Detection limits of major elements were under 0.01%. Detection limits of trace elements were provided in Table 4. Loss on ignition was not measured in either the dust or soil samples. The dust samples prepared for chemical analyses ranged from 30 to 100 mg in weight. The Cu, Ni, Pb, and Zn contents were measured only for 11 samples of enough sample weights.

4 Results

4.1 Mineralogy

4.1.1 Asian dust mineralogy

The mineral compositions of Asian dust determined by XRD are presented in Table 2. Five dusts were

independently quantified by SEM-EDS single-particle analyses. The XRD data are in good agreement with the SEM-EDS data, particularly the quartz content, total clay minerals, and ratio of plagioclase to K-feldspar. The SEM-EDS data support the reliability of the XRD quantifications (Table 2). However, the SEM-EDS analyses somewhat underestimated the K-feldspar, amphibole, and gypsum contents. This underestimation was due to ambiguity in the interpretation of the EDS patterns of some of the dust particles that are normally present as mixtures of several minerals. For example, K-feldspar is difficult to recognize from the mixture particle of K-feldspar and ISCMs because both K and Al are major constituents of two phases. Amphibole is difficult to distinguish unambiguously from the mixture particle of ISCMs and calcite. Distinguishing between calcite and gypsum in a mixture is also difficult. Thus, XRD quantification is probably more reliable than SEM-EDS quantification.

Clay minerals accounted for an average of 48% of the total mineral content. ISCMs were the major clay mineral (42% on average), followed by chlorite (4%) and kaolinite (2%) (Table 2). Although ISCMs also contained smectite, they were dominated by illite and illite-smectite mixed layers. A weak peak corresponding to expanded smectite was detected by XRD analysis of ethylene glycol treatment (Jeong, 2008; Park and Jeong, 2016). XRD analysis of clay minerals (< 2 μm) of the Chinese loess, which is a deposit of Asian dust, confirmed that clays are dominated by illite and illite-smectite mixed-layer minerals, with only minor amounts of smectite (Jeong et al., 2008).

The quartz content of dust samples was around 20%. Samples of very coarse dust from a 2012 dust event (D10–11) (Fig. 2) showed the highest quartz and lowest clay mineral content (Table 2). The average feldspar (plagioclase and K-feldspar) content was 18%. The average ratio of plagioclase (12.4%) to K-feldspar (5.1%) content was 2.5. Amphibole was detected as a minor mineral (2% on average).

Carbonates and gypsum are important constituents of dust because of their reactivity and solubility. The average content of calcite was 5%, but varied widely between 0.5 and 11%. The average content of gypsum was 5%, but this also varied widely, between 0.2 and 18.3%. Dolomite was a minor component, being present in proportions of around 1%. A small quantity of halite was detected only in a dust sample collected in Deokjeok Island (D17) during the 2015 dust event. Although iron oxides (goethite and hematite) are minor minerals (~ 1–2%) responsible for the yellow-brown color of dust, they were not quantified due to their low crystallinity.

4.1.2 Temporal variation of Asian dust mineralogy

Fig. 4 shows the temporal variation of mineral content in the dust samples. The clay mineral content varied in the opposite direction to the quartz and feldspar contents. Quartz-rich dust (D11) was sampled during the coarse dust event. The quartz, feldspar, and clay mineral contents do not show any significant

correlations with calcite and gypsum contents.

Three sets of intra-event dust samples (sets 1, 5, and 6 in Fig. 4) were collected at the same site. Set 1 samples showed little intra-event variation, while set 6 samples showed clear increases in clay and gypsum contents toward the end of the dust event, along with decreases in quartz, feldspar, and calcite contents. Set 5 samples showed a decrease of clay-mineral content, but with no notable change in quartz content.

The other sets of dust samples (sets 2–4 in Fig.4) were collected at different sites during the same dust event, and showed little spatial variation in mineral composition. However, in set 3, the gypsum content in samples from Deokjeok Island (D14) was far higher compared to samples from Andong (D13).

4.1.3 Soil mineralogy

The mineral compositions of surface soils (<20 μm) in the Mongolian Gobi Desert are presented in Supplementary Table S1. The mineral compositions varied among samples, probably according to the local geology. The total clay mineral content ranged widely among samples, from 25.3% (G18) to 67.4% (G34). This range was wider than that among the dust samples (33.8~59.1%). Clay minerals are dominated by ISCMs, followed by chlorite (4.3%) and kaolinite (3.0%). XRD analyses of clays (< 2 μm) treated with ethylene glycol revealed variation of the smectite content (Supplementary Fig. S2). Although some sample was enriched with smectite (sample G34), the XRD intensities of smectite were generally weak; illite and illite-smectite mixed layers tended to dominate ISCMs. The quartz content varied widely among samples, from 8.8% (G34) to 32.1% (G18). The average ratio of plagioclase (14.3%) to K-feldspar (5.5%) was approximately 2.6. Calcite contents were 9.5% on average. Soil samples G2, G19, and G28 exhibited calcite enrichment (> 20%). The calcite-rich samples are abundant in limestone pebbles (G2), and secondary calcite precipitates (G19 and G28). Gypsum was a minor component of source soils (0.6% on average), but was more abundant in samples G22 (5.6%) and G31 (3.2%) from dry lake beds, and in sample G25 (4.4%) from a dry river bed.

4.1.4 Comparison of mineralogy between Asian dust and soil samples

Mineral compositions are compared between the source soils and Asian dust samples in the box-whisker plots shown in Fig. 5. The plots show similar ranges of mineral contents between the Asian dust and source soil samples. Calcite and gypsum contents, however, differed between dust and soil samples. In source soils, gypsum was present only in trace amounts (average content of 0.6%), while calcite was

abundant (average content of 9.5%) (Supplementary Table S1, Fig. 5). In the dust samples, however, the average gypsum content was 5%, while the average calcite content was 5.1% (Table 2, Fig. 5).

4.2 Geochemistry

4.2.1 Comparison of geochemistry between Asian dust and soil samples

The major-element compositions of dust samples were recalculated on a volatile-free basis and are presented as metal wt% values (Table 3). Trace element compositions of dust samples are listed in Table 4. The major and trace element compositions of the source soil samples are listed in Supplementary Tables S2 and S3, respectively. The contents of major and trace elements of Asian dust and source soil samples were normalized by the average values for the upper continental crust (UCC) (Rudnick and Gao, 2003) and are presented in Figs. 6–8.

Major-element compositions of both the dust and soil samples did not coincide with the average UCC values (enrichment factor = 1). Si and Na were relatively depleted in dust and soils, compared with the average UCC (enrichment factor < 1), while Al, Fe, Mn, Mg, Ca, K, Ti, and P were relatively enriched in dust and soils (enrichment factor > 1) (Fig. 6). In general, the range of the major-element contents of Asian dust samples coincided with those of source soils (Fig. 6). However, Al, Fe, Mn, Mg, K, and P were slightly enriched in dust in comparison to soils. The ranges of Al, Fe, K, and Ti contents of dust samples were narrower than those of source soils. The ranges of Ca and Na contents were wide in both the dust and soil samples.

The UCC-normalized trace element composition data showed that dust samples were significantly enriched with Cu, Zn, Sn, Pb, and S relative to the source soil samples (Fig. 7). The dust samples were slightly enriched with Cr, Co, Ni, Sb, and Ba relative to the soil samples, while Sr, Y, Zr, Hf, and Ta were slightly depleted in dust (Fig. 7). Compared with the soil samples, the rare earth elements (REEs) of dust indicated systematic depletion of heavy REEs (Tb–Lu) relative to light REEs (La–Nd) (Fig. 8). The contents of V, Ga, Th, and U showed little difference between the dust and soil samples.

4.2.2 Temporal variation of Asian dust geochemistry

Time-series data of UCC-normalized major element contents are provided in Fig. 9. The Si, Al, Fe, and Ti contents showed little fluctuation within an enrichment factor of +/– 0.5. However, Ca, Mg, and Na contents exhibited large fluctuations over time.

Time-series data of UCC-normalized trace element contents showed that REEs and Zr exhibited

small variations around an enrichment factor of 1, whereas Sn fluctuated significantly (Fig. 10). Analyses of Cu, Zn, and Pb were carried out only for 11 samples (Table 4), due to limited sample quantity, and not shown in Fig. 10. Their enrichment factors varied greatly, between 1 and 100.

5 Discussion

5.1 Source of Asian dust

Previous backward trajectory analysis (Jeong, 2008) and satellite remote sensing data (Husar et al., 2001; Zhang et al., 2003; Xuan et al., 2004; Seinfeld et al., 2004; McKendry et al., 2008; Jeong, et al., 2014) indicated that Mongolian and northern Chinese deserts are the source of Asian dust transported to Korea. The satellite images of dust in this study confirmed that most dust outbreaks occurred in the Gobi Desert and sandy deserts distributed from southern Mongolia to northern China (Fig. 1a). The Taklamacan Desert is another source of Asian dust west of the Gobi Desert (Zhang, et al., 2003; Xuan et al., 2004). Unfortunately, the Taklamakan Desert, was not included in the available satellite images. Although Fig. 1a and Supplementary Fig. 1 are based on only one satellite image for the outbreak of each dust event, serial images acquired at an interval of 1 h or below around dust outbreaks revealed no notable migration of dust storms from the west of the Gobi Desert. Mineral compositions of Asian dust coincided with fine (<20 μm) surface soils sampled in the Mongolian Gobi Desert (Fig. 5). Lower calcite and higher gypsum contents are attributed to atmospheric reactions. Major element compositions of Asian dust also coincided with those of Mongolian Gobi Desert soils (Fig. 6).

Geochemical properties of Asian dust and Mongolian Gobi soils were compared with those of Taklamakan Desert soils in previous works (Honda and Shimizu, 1998; Honda et al., 2004; Jiang and Yang, 2019). The low Al, Fe, and K concentrations of the Taklamakan soils indicated low contents of clay minerals in comparison to those of Asian dust and Gobi soils, while the high Ca concentration indicated the enrichment of calcite in the Taklamakan soils (Fig. 6). Chemical index of alteration (CIA) (Nesbitt and Young, 1982) was calculated using silicate CaO (Tables 3 and S2), and shown in A–CN–K diagram (Fig. 11a). The range of CIA of Asian dust was consistent with the range of Gobi soils, but clearly distinguished from that of Taklamakan soils (Fig 11a). This indicated the enrichment of illitic clay minerals in Asian dust and Gobi soils derived from clay-rich bedrocks. Th–Sc–La and Th–Sc–Zr/10 discrimination diagrams by Bhatia and Crook (1986) showed that both the Asian dust and Gobi soils were majorly derived from the source rocks formed in the tectonic setting of continental island arc, while the Taklamakan soils from the source rocks in the setting of passive margin (Figs. 11b and c). The

Cs/K–Cs/Rb plot showed a discrimination of Taklamakan soils from both the Asian dust and Gobi soils (Fig. 11d). Since Cs is almost partitioned to illitic clay minerals (Derkowski and McCarty, 2017), fine fractions of Mongolian Gobi soils were enriched in illitic clay minerals relative to those of the Taklamakan desert. The properties of major and trace element compositions suggested that the Taklamakan Desert was not the source of Asian dust observed in Korea. There is some limitation due to differences in the size fractions of the samples analyzed by investigators. Nevertheless, the geochemical data of < 20 μm fraction in the Mongolian Gobi soils were consistent with those of < 63 μm fractions in this study (Fig. S3).

5.2 Path dependence of Asian dust geochemistry

Large temporal variation of Ca contents is a prominent feature of Asian dust, in contrast to the small variations in Fe, Ti, K, Al, and Si contents (Fig. 9). Mg and Na contents also varied significantly, and showed positive correlations with Ca content (Fig. 9, Supplementary Fig. S4). Migration path data of the individual dust event in Supplementary Fig. S1 showed that Ca content is associated with the migration path of Asian dust. In total, 40% of the Asian dust storms migrating to the Korean Peninsula crossed the Chinese Loess Plateau (D3–6, D7, D10–11, D12, D19–20, and D21–23 in Fig. 9). All of the dust storms passing over the Loess Plateau were enriched with Ca (enrichment factor > 2.0 in Fig. 9).

Potential origins of the high-Ca dust storm are proposed here. The first is the entrainment of dust particles from the Loess Plateau. Although most dust storms originate from the deserts northwest of Loess Plateau, the storms may continuously entrain fine particles from the Loess Plateau in their early stages, i.e., just after leaving the desert. Loess is a loose eolian sediment comprising fine silt particles, and is probably susceptible to wind erosion. The average UCC-normalized Ca content of source soil samples (Table S2), excluding three outliers (G2, G19, and G28), was 2.2 versus 2.7–2.9 for loess (Jeong et al., 2008, 2011). Abundant pedogenic calcite was derived via the dissolution of primary calcite in climates wetter than desert (Jeong et al., 2008, 2011). In addition, the satellite image showed a dust outbreak over Loess Plateau in 2013 (D12) (Supplementary Fig. S1). However, the mass emission of dust particles from the Loess Plateau is contradictory to current understanding. Most observation and dust emission modeling data showed that the Chinese Loess Plateau is a major sink for, but a very minor source of, dust (Zhang et al., 2003; Xuan et al., 2004).

The second potential origin of the high-Ca dust storm is the sandy deserts of northern China, which are distributed between the Mongolian Gobi Desert and the Loess Plateau. The mineralogy and geochemistry of fine soil fractions of the Mongolian Gobi Desert (Supplementary Tables S1–3) and the Loess Plateau (Supplementary Table S4) have been well characterized in this study and previous work

(Jahn et al., 2001). However, the fine soil fractions of the sandy deserts lying between the Gobi Desert and the Loess Plateau were not investigated in this study and have rarely been addressed in previous works. The Gobi Desert ranges from southern Mongolia to northern China and is covered with silt, sand, gravel, rocky outcrops, and sparse vegetation with scattered dunes; in contrast, the sandy deserts in northern China (Badain Jaran, Tengger, Wulanbuhe, Kubuqi, and Maowusu deserts) are covered with dune fields. Subsaline to hypersaline and dry lakes are particularly common in the interdune basin of the Badain Jaran and Tengger deserts (Yang et al., 2003; Yang et al., 2011). Na, Ca, and Mg are the major cations in the hypersaline lake waters. Calcareous cementation is common on the surfaces of paleodunes. Calcareous lacustrine sediments deposited when the lake level was high are distributed around lakes and dry basins (Yang et al., 2003). Calcareous cements and deposits composed of soft carbonate minerals are vulnerable to sand blasting occurring during dust storms, which supplies calcareous dust to migrating storms. A fraction of Mg and Na may also be present in the form of carbonates. In this study, XRD analyses of the samples from dust events that passed over the Loess Plateau revealed a weak peak corresponding to natron ($Na_2CO_3 \cdot 10H_2O$). The role of the sandy desert of northern China in the major element composition of Asian dust merits further investigation.

In this stage of research, the origin of high-Ca dust storm cannot be fully resolved because analytical data are insufficient, particularly in the sandy deserts of northern China. The origin of high-Ca dust could be clarified by further mineralogical and geochemical investigation of the sandy deserts and the estimation on the possibility of dust emission from loess plateau.

5.3 Fractionation of minerals in dust

The mineral compositions of the dust samples were generally consistent with those of source soils, indicating that little mineralogical fractionation occurred during dust storm outbreak and migration. It is noted that the coarsest dust (D11) was enriched with quartz and feldspars but relatively depleted in clay minerals. The dust samples for one individual event (set 6; see Fig. 4) showed systematic changes in mineral contents, i.e., increasing clay mineral content and decreasing quartz and feldspar contents, toward the end of the dust event. The temporal changes in the mineralogy of the set 6 samples (D21–23) appear to be attributable to a decrease in particle size. Size distribution curves in Fig. 2 show the gradual decrease of coarse fractions (> 10 μm) from D21 to D23. In samples of sets 1 and 5, temporal changes of mineral composition were not evident and difficult to explain. These may be related to the meteorological conditions during storm outbreak, migration, gravity settling, mixing or cloud processing. Mineral compositions of dust collected at different sites during individual events (sample sets 2–4; see Fig. 4) showed no obvious differences among sites, indicating that Korean Peninsula is

likely too narrow to exhibit spatial variation of Asian dust properties.

5.4 Fractionation of trace elements between soils and dust

The ranges of the major element contents of the Asian dust samples were consistent with those of source soils, while trace elements in the dust were fractionated from soils, showing lower Y, Zr, Hf, Ta, and heavy REE contents (Figs 7 and 8). Preferential depletion of heavy REEs suggests depletion of zircon, which is a mineral known to host heavy REEs (Henderson, 1984). Gravity settling of trace heavy minerals, particularly zircon, during the migration may be responsible for the fractionation of trace elements between soil and dust.

The chondrite-normalized $(La/Yb)_N$ ratio (chondrite values by Boynton (1984)) represents the fractionation of heavy REEs from light REEs. The average $(La/Yb)_N$ ratio of Asian dust in this study was 11.6, which was considerably higher than that of the source soil samples (8.7), probably due to the depletion of heavy REE-rich zircon. Meanwhile, the average europium (Eu) anomaly of dust (0.71) was not different from that of soil (0.70), which showed little fractionation (Table 4 and Supplementary Table S3) because Eu is hosted by plagioclase. The Chinese Loess Plateau is a sink of Asian dust neighboring on deserts. The $(La/Yb)_N$ ratio of Chinese loess are 8.7 in this study (average for 44 samples) (Supplementary Table S4) and 9.0 in Jahn et al. (2001; average for 30 samples) (Supplementary Table S5). The Eu anomaly for the Chinese loess showed little fractionation (0.65 in this study, and 0.64 in Jahn et al., 2001) from soils (0.70). These data indicate that Asian dust deposited on the Loess Plateau neighboring on the dust source experienced little fractionation.

Analytical data of REE compositions are rare to find in previous works on Asian dust transported over long distances. Lee et al. (2010) measured REEs in Asian dust sampled at three sites, derived from a dust event that took place in Korea during the period April 24–25, 2006. The average $(La/Yb)_N$ and Eu/Eu* ratios recalculated based on from their REE data were 11.5 and 0.55, respectively (Supplementary Table S6). The $(La/Yb)_N$ ratio obtained by Lee et al. (2010) is consistent with the values obtained in this study, although the Eu anomaly is somewhat low. The REE contents of Asian dust originated from the Gobi Desert and transported to the St. Elias Mountains (Yukon Territory, Canada) were reported by Zdanowicz et al. (2007). The $(La/Yb)_N$ and Eu/Eu* ratios calculated based on the six REE data in the Yukon dust (excluding local dust) are 11.1 and 0.65, respectively (Supplementary Table S6), which are consistent with those for Korean dust. These findings support that the geochemical and mineralogical characteristics of Asian dust sampled in the Yukon Territory were little different from the dust sampled in Korea. Remarkably, the modal volume diameters of Asian dust particles are uniform among samples collected at the western margin of the North Pacific (this study), in North Pacific Ocean

sediments (Serno et al., 2014), and in the subarctic mountains of the North America (Zdanowicz et al., 2007). Previous studies showed that dust did not show significant changes in size distribution beyond transport distance of ~2,000 km, (Nakai et al., 1993; Rea,1994; Rea and Hovan,1995; Serno et al., 2014). Rather uniform properties of trans-Pacific Asian dust indicate that REE fractionation of Asian dust occurred in a distance of ~ 2000 km from sources.

Deep-sea sediment samples from the central North Pacific Ocean were investigated in terms of REE contents to elucidate paleoclimatic changes. Since the sediments are normally mixtures of local volcanogenic particles and long-range transport eolian dust from Asia, the Chinese loess (and related sediments) are usually selected as an endmember of eolian component to estimate the accumulation rate and provenance of eolian particles. The $(La/Yb)_N$ ratios of Asian dust fractions separated from pelagic sediments from the North Pacific were recorded as 9.1 (three central North Pacific samples, Nakai et al., 1993), 7.3 (11 samples from southern transect, Serno et al., 2014), and 7.7 (type 1 samples, Hyeong et al., 2004) (Supplementary Tables S7). These values are much lower than those of the Asian dust transported long distances in Zdanowicz et al. (2007), Lee et al. (2010), and this study. The Eu anomaly of pelagic sediments (0.66, Nakai et al. 2004; 0.74, Hyeong et al. 2004; 0.73, Serno et al. 2014) (Supplementary Tables S7) is similar to that of Asian dust (0.71, this study; 0.65, Zdanowicz et al., 2007). REE data on long-range transport Asian dust in this study may improve the usefulness of REE as a proxy of paleoclimatic change.

5.5 Mixing and reaction of Asian dust with polluted air

Asian dust passes through industrialized regions of East Asia, where air pollution is a severe environmental issue. Asian dust mixes and reacts with polluted air (Nishikawa et al., 1991; McKendry, et al., 2008; Huang et al., 2010). The concentration of atmospheric pollutants is high particularly in winter and spring seasons which are also the major seasons of dust outbreaks. Calcite, which is the most reactive mineral in dust, reacts with acidic gases in the atmosphere (mostly sulfur species) originating from pollution (Dentener et al., 1996; Laskin et al., 2005; Matsuki et al., 2005; Jeong and Chun, 2006; Takahashi et al., 2009, 2014). Higher gypsum and lower calcite contents of Asian dust compared to source soils (Table 2, Supplementary Table S1, and Fig. 5) suggest the conversion of calcite into gypsum during the transport (Takahashi et al., 2009, 2014). This conversion is also supported by the similar average Ca contents of both the dust (5.1%) and soils (6.4%). During one of the individual dust events in this study (set 6 samples; see Fig. 4), the increased gypsum content and concomitantly decreased calcite content were clearly the result of progressive reaction of dust with air pollutants toward the end of the dust event. During the dust event of set 3, the gypsum content of dust was greatly enhanced

concomitantly with the decrease of calcite content at Deokjeok Island (D14), while it was lower than the calcite content at Andong (D13). This supports the conversion of calcite to gypsum in the severely polluted atmosphere around the densely populated metropolitan region of Seoul, Korea. Marked variation of both the calcite (0.5~11%) and gypsum (0~18%) contents of dust is intuitive because pollutant concentrations vary widely with regional weather conditions.

In Asian dust, Cu, Zn, Sn, and Pb (Fig. 7) are the major heavy metal pollutants of combustion origin (Duan and Tan, 2013). Although the contents of Cu, Zn, and Pb were not analyzed in all of the samples due to small dust quantities, the marked temporal variation of Sn content represent the temporal variation of heavy metal pollutants (Fig. 10). The intra-event dust samples of set 6 showed a gradual increase of Sn content toward the end of the dust event, while the contents of REEs and Zr of soil origin decreased progressively, consistent with progressive mixing of dust with regional pollutants (Fig. 10). The Sn contents were low in samples of sets 2 and 4, showing only minor variations, but it was high in D14 (set 3) at Deokjeok Island, consistent with high gypsum content.

6 Summary and Conclusions

Systematic analyses of Asian dust samples collected over a long period showed the mineralogical and geochemical properties consistent with those of fine silt fractions (< 20 μm) of the source soils. Clay minerals were most abundant, followed by quartz, plagioclase, K-feldspar, calcite, and gypsum. Asian dust crossing the Loess Plateau has a higher Ca content, entraining calcite-rich fine dust particles that probably originated from calcareous sediments in northern China sandy deserts and pedogenic calcite-rich loess. Dust-laden air parcels mix with atmospheric pollutants over East Asia. Calcite was found to react with pollutants to form gypsum. Serial dust samples for each dust event show scant changes in major-element contents. However, trace element contents varied widely due to REE fractionation and mixing with polluted air enriched with heavy metals of pollution origin. Selective depletion of heavy REEs in dust from source soils resulted in increased $(La/Yb)_N$ ratios. The samples of one dust event showed a trend of increasing clay minerals and gypsum contents toward the end of the event in association with decreasing particle size and progressive reactions. Mineral dust transported over long distances is the subject of much interdisciplinary research. This study describes not only the average properties of dust, but also inter-event variations therein and fractionation from source soils, thereby providing a basis for climatic and atmospheric reaction modeling, and for analysis of deep-sea sediments, fine-grained soils, and ice-sheet dust.

Acknowledgements

This study was funded by the National Research Foundation of Korea grant NRF-2017R1A2B2011422 to G.Y. Jeong.

References

An, Z. S., Kukla, G., and Porter, S. C.: Magnetic susceptibility evidence of Monsoon variation on the loess plateau of central China during the last 130,000 years, Quaternary Res., 36, 29–36, 1991.

Bautista-Tulin, A. T. and Inoue, K.: Hydroxy-interlayered minerals in Japanese soils influenced by eolian deposition, Soil Sci. Soc. Am. J., 61, 631–640, 1997.

Bhatia, M. R. and Crook, A. A. W.: Trace element characteristics of graywackes and tectonic setting discrimination of sedimentary basins, Contrib. Mineral Petrol, 92, 181–193, 1986.Biscaye, P. E., Grousset, F. E., Revel, M., Van der Gaast, S., Zielinski, G. A., Vaars, A., and Kukla, G.: Asian provenance of glacial dust (stage 2) in the Greenland Ice Sheet Project 2 Ice Core, Summit, Greenland, J. Geophys. Res., 102, 26765–26781, 1997.

Bory, A. J. -M., Biscaye, P. E., Svensson, A., and Grousset, F. E.: Seasonal variability in the origin of recent atmospheric mineral dust at North GRIP, Greenland. Earth Planet Sci. Lett., 196, 123–134, 2002.

Boynton, W. V.: Geochemistry of the rare earth elements: meteorite studies: Rare Earth Element Geochemistry, edited by Henderson, P., Elsevier, printed in Netherlands, 1984.

Chen, J., Li, G., Yang, J., Rao, W., Lu, J., Balsam, W., Sun, Y., Ji, J.: Nd and Sr isotopic characteristics of Chinese deserts: implications for the provenances of Asian dust, Geochim. Cosmochim. Acta, 71, 3904–3914, 2007.

Chun, Y., Boo, K. -O., Kim, J., Park, S. -U., and Lee, M.: Synopsis, transport, and physical characteristics of Asian dust in Korea, J. Geophys. Res.-Atmos., 106, 18461–18469, 2001.

Dentener, F. J., Carmichael, G. R., Zhang, Y., Lelieveld, J., and Crutzen, P. J.: Role of mineral aerosol as a reactive surface in the global troposphere, J. Geophys. Res., 101, 22869–22889, 1996.

Derkowski, A. and McCarty, D. K.: Cesium, a water-incompatible, siloxane-complexed cation in Earth's upper crust, Geology, doi:10.1130/G39150.1, 2017.

Duan, J. and Tan, J.: Atmospheric heavy metals and Arsenic in China: Situation, sources and control policies, Atmos. Environ., 74, 93–101, 2013.

Ferrat, M., Weiss, D. J., Strekopytov, S., Dong, S. F., Chen, H. Y., Najorka, J., Sun, Y. B., Gupta, S., Tada, R., and Sinha, R.: Improved provenance tracing of Asian dust sources using rare earth elements and selected trace elements for palaeomonsoon studies on the eastern Tibetan Plateau,

576 Geochim. Cosmochim. Acta, 75, 6374–6399, 2011.
577 Formenti, P., Schütz, L., Balkanski, Y., Desboeufs, K., Ebert, M., Kandler, K., Petzold, A., Scheuvens,
578 D., Weinbruch, S., and Zhang, D.: Recent progress in understanding physical and chemical
579 properties of African and Asian mineral dust, Atmos. Chem. Phys., 11, 8231–8256,
580 doi:10.5194/acp-11-8231-2011, 2011.
581 Forster, P., Ramaswamy, V., Artaxo, P., Berntsen, T., Betts, R., Fahey, D. W., Haywood, J., Lean, J.,
582 Lowe, D. C., Myhre, G., Nganga, J., Prinn, R., Raga, G., Schulz, M., and Van Dorland, R.: Changes
583 in Atmospheric Constituents and in Radiative Forcing, in: Climate Change 2007: The Physical
584 Science Basis, Contribution of Working Group I to the Fourth Assessment Report of the
585 Intergovernmental Panel on Climate Change, edited by Solomon, S., Qin, D., Manning, M., Chen,
586 Z., Marquis, M., Averyt, K. B., Tignor, M., and Miller, H. L., Cambridge University Press, printed
587 in United Kingdom, 2007.
588 Henderson, P.: General geochemical properties and abundances of the rare earth elements: Rare Earth
589 Element Geochemistry, edited by Henderson, P., Elsevier, printed in Netherlands, 1984.
590 Honda, M. and Shimizu, H.: Geochemical, mineralogical and sedimentological studies on the
591 Taklimakan Desert sands, Sedimentology, 45, 1125–1143, 1998.
592 Honda, M., Yabuki, S., and Shimizu, H.: Geochemical and isotopic studies of Aeolian sediments in
593 China, Sedimentology, 51, 211–230, 2004.
594 Huang, K., Zhuang, G., Li, J., Wang, Q., Sun, Y., Lin, Y., and Fu, J. S.: Mixing of Asian dust with
595 pollution aerosol and the transformation of aerosol components during the dust storm over China
596 in spring 2007, J. Geophys. Res., 115, D00K13, doi:10.1029/2009JD013145, 2010.
597 Husar, R. B., Tratt, D. M., Schichtel, B. A., Falke, S. R., Li, F., Jaffe, D., Gassó, S., Gill, T., Laulainen,
598 N. S., Lu, F., Reheis, M. C., Chun, Y., Westphal, D., Holben, B. N., Gueymard, C., McKendry, I.,
599 Kuring, N., Feldman, G. C., McClain, C., Frouin, R. J., Merrill, J., DuBois, D., Vignola, F.,
600 Murayama, T., Nickovic, S., Wilson, W. E., Sassen, K., Sugimoto, N., and Malm, W. C.: Asian
601 dust events of April 1998, J. Geophys. Res.-Atmos., 106, 18317–18330, 2001.
602 Hyeong, K., Park, S. -H., Yoo, C. M., and Kim, K. -H.: Mineralogical and geochemical compositions
603 of the eolian dust from the northeast equatorial Pacific and their implications on paleolocation of
604 the Intertropical Convergence Zone, Paleoceanography, 20, PA1010, doi:10.1029/2004PA001053,
605 2005.
606 Jahn, B. M., Gallet, S., and Han, J. M.: Geochemistry of the Xining, Xifeng and Jixian sections, Loess
607 Plateau of China: eolian dust provenance and paleosol evolution during the last 140 ka, Chem.
608 Geol., 178, 71–94, 2001.
609 Jiang, Q. and Yang, X.: Sedimentological and geochemical composition of aeolian sediments in the

610 Taklamakan Desert: implications for provenance and sediment supply mechanisms, J. Geophys.
611 Res.-Earth Surface, 124, 1217–1237, https://doi.org/10.1029/2018JF004990, 2019.
612 Jickells, T. D., An, Z. S., Andersen, K. K., Baker, A. R., Bergametti, G., Brooks, N., Cao, J. J., Boyd,
613 P. W., Duce, R. A., Hunter, K. A., Kawahata, H., Kubilay, N., laRoche, J., Liss, P. S., Mahowald,
614 N., Prospero, J. M., Ridgwell, A. J., Tegen, I., and Torres, R.: Global iron connections between
615 desert, dust, ocean biogeochemistry, and climate, Science, 308, 67–71, 2005.
616 Jeong, G. Y.: Bulk and single-particle mineralogy of Asian dust and a comparison with its source soils,
617 J. Geophys. Res.-Atmos., 113, D02208, doi:10.1029/2007JD008606, 2008.
618 Jeong, G. Y. and Achterberg, E. P.: Chemistry and mineralogy of clay minerals in Asian and Saharan
619 dusts and the implications for iron supply to the oceans, Atmos. Chem. Phys., 14, 12415–12428,
620 doi:10.5194/acp-14-12415-2014, 2014.
621 Jeong, G. Y. and Chun, Y.: Nanofiber calcite in Asian dust and its atmospheric roles, Geophys. Res.
622 Lett., 33, L24802, doi:10.1029/2006GL028280, 2006.
623 Jeong, G. Y. and Nousiainen, T.: TEM analysis of the internal structures and mineralogy of Asian dust
624 particles and the implications for optical modeling, Atmos. Chem. Phys., 14, 7233–7254,
625 doi:10.5194/acp-14-7233-2014, 2014.
626 Jeong, G. Y., Hillier, S., and Kemp, R. A.: Quantitative bulk and single-particle mineralogy of a thick
627 Chinese loess-paleosol section: implications for loess provenance and weathering, Quaternary Sci.
628 Rev., 37, 1271–1287, 2008.
629 Jeong, G. Y., Hillier, S., and Kemp, R. A.: Changes in mineralogy of loess-paleosol sections across the
630 Chinese Loess Plateau, Quaternary Res., 75, 245–255, 2011.
631 Jeong, G. Y., Choi, J. -H., Lim, H. S., Seong, C., and Yi, S. B.: Deposition and weathering of Asian
632 dust in Paleolithic sites, Korea, Quaternary Sci. Rev., 78, 283–300, 2013.
633 Jeong, G. Y., Park, M. Y., Kandler, K., Nousiainen, T., and Kemppinen, O.: Mineralogical properties
634 and internal structures of individual fine particles of Saharan dust, Atmos. Chem. Phys., 16,
635 12397–12410, 2016, doi:10.5194/acp-16-12397-2016, 2016.
636 Jeong, G. Y., Kim, J. Y., Seo, J., Kim, G. M., Jin, H. C., and Chun, Y.: Long-range transport of giant
637 particles in Asian dust identified by physical, mineralogical, and meteorological analysis, Atmos.
638 Chem. Phys., 14, 505–521, doi:10.5194/acp-14-505-2014, 2014.
639 Jickells, T. D., An, Z. S., Andersen, K. K., Baker, A. R., Bergametti, G., Brooks, N., Cao, J. J., Boyd,
640 P. W., Duce, R. A., Hunter, K. A., Kawahata, H., Kubilay, N., laRoche, J., Liss, P. S., Mahowald,
641 N., Prospero, J. M., Ridgwell, A. J., Tegen, I., and Torres, R.: Global iron connections between
642 desert, dust, ocean biogeochemistry, and climate, Science, 308, 67–71, 2005.
643 Jo, H. -Y., Jeong, G. Y., and Park, M. Y.: Mineralogy, geochemistry, and eolian source of mountain soils

644 on quartzite. J. Geol. Soc. Korea, 55, 87–103(in Korean with English abstract), 2019.
645 Johnson, M. S. and Meskhidze, N.: Atmospheric dissolved iron deposition to the global oceans: effects
646 of oxalate-promoted Fe dissolution, photochemical redox cycling, and dust mineralogy, Geosci.
647 Model Dev., 6, 1137–1155, doi:10.5194/gmd-6-1137-2013, 2013.
648 Kanayama, S., Yabuki, S., Yanagisawa, F., and Motoyama, R., 2002, The chemical and strontium
649 isotope composition of atmospheric aerosols over Japan: the contribution of long-range-
650 transported Asian dust (Kosa), Atmos. Environ., 36, 5159–5175.
651 Korea Meteorological Administration: Portal Opening Meteorological Data,
652 https://data.kma.go.kr/cmmn/main.do, 2019.
653 Krueger, B. J., Grassian, V. H., Cowin, J. P., and Laskin, A.: Heterogeneous chemistry of individual
654 mineral dust particles from different dust source regions: the importance of particle mineralogy,
655 Atmos. Environ., 38, 6253–6261, 2004.
656 Laskin, A., Wietsma, T. W., Krueger, B. J., and Grassian, V. H.: Heterogeneous Chemistry of Individual
657 Mineral Dust Particles with Nitric Acid: A Combined CCSEM/EDX, ESEM, and ICP-MS Study,
658 J. Geophys. Res.-Atmos., 110, D10208, doi:10.1029/2004JD005206, 2005.
659 Lee, M. K., Lee, Y. I., and Yi, H. I.: Provenances of atmospheric dust over Korea from Sr–Nd isotopes
660 and rare earth elements in early 2006, Atmos. Environ., 44, 2401–2414, 2010.
661 Leinen, M., Prospero, J. M., Arnold, E., and Blank, M.: Mineralogy of Aeolian dust reaching the North
662 Pacific Ocean 1. Sampling and analysis, J. Geophys. Res.-Atmos., 99, D10, 21017–21023, 1994.
663 Liu, T. S., et al.: Loess in China, China Ocean Press, Springer-Verlag, printed in Germany, 1988.
664 Maher, B. A., Mutch, T. J., and Cunningham, D.: Magnetic and geochemical characteristics of Gobi
665 Desert surface sediments: implications for provenance of the Chinese loess, Geology, 37, 279–282,
666 2009.
667 Mahowald, N. M. and Kiehl, L. M.: Mineral aerosol and cloud interaction, Geophys. Res. Lett., 30,
668 1475, doi10.1029/2002GL016762, 2003.
669 Martin, J. H. and Fitzwater, S. F.: Iron deficiency limits phytoplankton growth in the north-east Pacific
670 subarctic, Nature, 331, 341–342, 1988.
671 Matsuki. A., Iwasaka, Y., Shi, G., Zhang, D., Trochkine, D., Yamada, M., Kim, Y. -S., Chen, B.,
672 Nagatani, T., Miyazawa, T., Nagatani, M., and Nagata, H.: Morphological and chemical
673 modification of mineral dust: Observational insight into the heterogeneous uptake of acidic gases,
674 Geophys. Res. Lett., 32, L22806, doi:10.1029/2005GL024176, 2005.
675 McGee, D., Winckler, G., Borunda, A., Serno, S., Anderson, R. F., Recasens, C., Bory, A., Gaiero, D.,
676 Jaccard, S. L., Kaplan, M., McManus, J. F., Revel, M., and Sun, Y.: Tracking eolian dust with
677 helium and thorium: Impacts of grain size and provenance, Geochim. Cosmochim. Acta, 175, 47–

678 67, 2016.
679 McKendry, I. G., Macdonald, A. M., Leaitch, W. R., van Donkelaar, A., Zhang, Q., Duck, T., and
680 Martin, R. V.: Trans-Pacific dust events observed at Whistler, British Columbia during INTEXB,
681 Atmos. Chem. Phys., 8, 6297–6307, doi:10.5194/acp-8-6297-2008, 2008.
682 Meskhidze, N., Chameides, W. L., and Nenes, A.: Dust and pollution: a recipe for enhanced ocean
683 fertilization, J. Geophys. Res., 110, D03301, doi:10.1029/2004JD005082, 2005.
684 Moore, D. M. and Reynolds, R.C., Jr.: X-ray diffraction and the identification and analysis of clay
685 minerals, Oxford University Press, printed in New York, 1997.
686 Nakai, S., Halliday, A. N., and Rea, D. K.: Provenance of dust in the Pacific Ocean, Earth Planet Sci.
687 Lett., 119, 143–157, 1993.
688 National Meteorological Satellite Center: http://nmsc.kma.go.kr/enhome/html/main/main.do (last
689 access: 16 September 2019), 2019.
690 Nesbitt, H. W. and Young, G. M. (1982) Early Proterozoic climates and plate motions inferred from
691 major element chemistry of lutite. Nature, 299, 715–717.
692 Nishikawa, M., Kanamori, S., Kanamori, N., and Mizoguchi, T.: Kosa aerosol as eolian carrier of
693 anthropogenic material, Sci. Total Environ., 107, 13–27, 1991.
694 Olivarez, A. M., Owen, R. M., and Rea, D. K.: Geochemistry of eolian dust in Pacific pelagic sediments:
695 Implications for paleoclimatic interpretations, Geochim. Cosmochim. Acta, 55, 2147–2158, 1991.
696 Park, M. Y. and Jeong, G. Y.: Mineralogical properties of Asian dust sampled at Deokjeok Island,
697 Incheon, Korea in February 22, 2015, J. Min. Soc. Korea, 29, 79–87 (in Korean with English
698 abstract), 2016.
699 Pettke, T., Halliday, A. N., Hall, C. M., and Rea, D. K.: Dust production and deposition in Asia and the
700 north Pacific Ocean over the past 12 Myr, Earth Planet Sci. Lett., 178, 397–413, 2000.
701 Porter, S. C.: Chinese loess record of monsoon climate during the last glacial-interglacial cycle, Earth-
702 Sci. Rev., 54, 115–128, 2001.
703 Rea, D. K.: The paleoclimatic record provided by eolian deposition in the deep sea: the geologic history
704 of wind, Rev. Geophys., 32, 159–195, 1994.
705 Rea, D. K. and Hovan, S. A.: Grain size distribution and depositional processes of the mineral
706 component of abyssal sediments: Lessons from the North Pacific, Paleoceanography, 10, 251–258,
707 1995.
708 Rea, D. K., Snoeckx, H., and Joseph, L. H.: Late Cenozoic eolian deposition in the North Pacific: Asian
709 drying, Tibetan uplift, cooling of the northern hemisphere, Paleoceanography, 13, 215–224, 1998.
710 Rudnick, R. and Gao, S.: Composition of the continental crust: The Crust, Treatise on Geochemistry,
711 vol. 3., edited by Rudnick, R.L., Elsevier–Pergamon, printed in Italy, 2003.

712 Seinfeld, J. H., Carmichael, G. R., Arimoto, R., Conant, W. C., Brechtel, F. J., Bates, T. S., Cahill, T.
713 A., Clarke, A. D., Doherty, S. J., Flatau, P. J., Huebert, B. J., Kim, J., Markowicz, K. M., Quinn,
714 P. K., Russell, L. M., Russell, P. B., Shimizu, A., Shinozuka, Y., Song, C. H., Tang, Y., Uno, I.,
715 Vogelmann, A. M., Weber, R. J., Woo, J. -H, and Zhang, X. Y.: ACE-ASIA regional climatic and
716 atmospheric chemical effects of Asian dust and pollution, B. Am. Meteorol. Soc., 85, 367–380,
717 2004.
718 Serno, S. S., Winckler, G., Anderson, R. F., Hayes, C. T., McGee, D., Machalett, B., Ren, H., Straub, S.
719 M., Gersonde, R., Haug, G. H.: Eolian dust input to the Subarctic North Pacific, Earth Planet Sci.
720 Lett., 387, 252–263, 2014.
721 Shi, Z., Shao, L., Jones, T. P., and Lu, S.: Microscopy and mineralogy of airborne particles collected
722 during severe dust storm episodes in Beijing, China, J. Geophys. Res., 110, D01303,
723 doi:10.1029/2004JD005073, 2005.
724 Takahashi, Y., Higashi, M., Furukawa, T., and Mitsunobu, S.: Change of iron species and iron solubility
725 in Asian dust during the long-range transport from western China to Japan, Atmos. Chem. Phys.,
726 11, 11237–11252, doi:10.5194/acp-11-11237-2011, 2011.
727 Takahashi, Y., Miyoshi, T., Higashi, M., Kamioka, H., and Kanai, Y.: Neutralization of calcite in
728 mineral aerosols by acidic sulfur species collected in China and Japan studied by Ca K-edge X-
729 ray absorption near-edge structure, Environ. Sci. Technol., 43, 6535–6540, 2009.
730 Takahashi, Y., Higashi, M., Furukawa, T., Miyoshi, T., Fujiwara, M., and Uematsu, M.: A study of the
731 chemical processes in aerosols and their impacts on the environment using X-ray absorption fine
732 structure spectroscopy, in Western Pacific Air-Sea Interaction Study, edited by Uematsu, M.,
733 Yokouchi, Y., Watanabe, Y. W., Takeda, S., and Yamanaka, Y., TERRAPUB, printed in Japan,
734 doi:10.5047/w-pass.a01.005, 2014.
735 Xuan, J., Sokolik, I. N., Hao, J., Guo, F., Mao, H., and Yang, G.: Identification and characterization of
736 sources of atmospheric mineral dust in East Asia, Atmos. Environ., 38, 6239–6252, 2004.
737 Yang, X., Liu, T., and Xiao, H.: Evolution of megadunes and lakes in the Badain Jaran desert, Inner
738 Mongolia, China during the last 31000 years, Quaternary Int., 104, 99–112, 2003.
739 Yang, X., Scuderi, L., Paillou, P., Liu, Z., Li, H., and Ren, X.: Quaternary environmental changes in
740 the drylands of China – A critical review, Quaternary Sci. Rev., 30, 3219–3233, 2011.
741 Zdanowicz, C., Hall, G., Vaive, J., Amelin, Y., Percival, J., Girard, I., Biscaye, P., and Bory, A.: Asian
742 dustfall in the St. Elias Mountains, Yukon, Canada, Geochim. Cosmochim. Acta, 70, 3493–3507,
743 2007.
744 Zhang, X. Y., Gong, S. L., Zhao, T. L., Arimoto, R., Wang, Y. Q., and Zhou, Z. J.: Sources of Asian dust
745 and role of climate change versus desertification in Asian dust emission, Geophys. Res., Lett., 30,

2272, doi:10.1029/2003GL018206, 2003.

780

781

782

Table 1. List of Asian dust sampled in Korea and desert soils from Mongolian Gobi desert.

Asian dust							Mongolian Gobi desert soil		
Sample	Site[1)]	Year	Month/Date (sampling hour)	Tran[2)] (h)	Dist.[3)] (km)	Conc.[4)] (μg/m^3)	Sample	Latitude	Longitude
D1	AD	2005	4/20(09-17)	-	-	366	G1	N 45º 19' 21.39"	E 106º 32' 47.40"
D2	AD	2008	5/31(08-18)	54	1800	292	G2	N 44º 40' 39.67"	E 106º 56' 13.41"
D3	AD	2009	3/16(09-18)				G3	N 44º 26' 46.20"	E 107º 08' 21.72"
D4	AD	2009	3/16(18)-17(09)	45	1900	428	G4	N 44º 14' 17.02"	E 107º 32' 07.85"
D5	AD	2009	3/17(09-18)				G5	N 44º 04' 00.11"	E 107º 43' 32.88"
D6	AD	2009	3/17(19)-18(09)				G6	N 44º 04' 01.97"	E 108º 16' 22.73"
D7	AD	2010	3/20(19)-21(10)	30	2200	1788	G7	N 43º 37' 48.48"	E 108º 33' 42.42"
D8	AD	2011	5/1(09-18)	41	1300	300	G8	N 43º 27' 28.00"	E 109º 01' 39.26"
D9	AD	2011	5/12(20)-13(11)	49	1700	322	G9	N 43º 14' 50.26"	E 108º 10' 02.68"
D10	SL	2012	3/31(09)-4/1(08)	25	1700	215	G10	N 43º 11' 28.31"	E 107º 01' 11.78"
D11	DJ	2012	3/31(09)-4/1(08)			220	G11	N 42º 38' 16.75"	E 107º 18' 45.96"
D12	SL	2013	3/9(09)-10(08)	-	1500	215	G12	N 42º 32' 24.88"	E 106º 55' 27.65"
D13	AD	2014	3/18(10-22)	42	1800	378	G13	N 42º 32' 41.71"	E 106º 29' 27.33"
D14	DJ	2014	3/18(09-24)			214	G14	N 42º 28' 43.44"	E 106º 02' 20.82"
D15	SL	2015	2/22(09)-23(08)			1044	G15	N 42º 43' 57.89"	E 105º 28' 30.02"
D16	AD	2015	2/22(16)-23(18)	23	1400	469	G16	N 43º 06' 27.97"	E 104º 58' 05.30"
D17	DJ	2015	2/22(09)-23(08)			1037	G17	N 43º 05' 29.85"	E 104º 13' 29.36"
D18	AD	2015	3/1(17)-2(11)	29	1600	281	G18	N 42º 51' 36.78"	E 104º 08' 24.24"
D19	SL	2016	3/6(09)-7(08)	44	1700	168	G19	N 42º 31' 21.33"	E 103º 51' 15.57"
D20	SL	2016	3/7(09)-8(08)				G20	N 42º 43' 41.69"	E 103º 45' 58.64"
D21	AD	2017	5/6(13-21)				G21	N 42º 52' 35.91"	E 103º 46' 44.04"
D22	AD	2017	5/6(21)-7(19)	60	1700	331	G22	N43º 10' 52.04"	E 104º 00' 38.56"
D23	AD	2017	5/8(14)-9(10)				G23	N 43º 21' 00.20"	E 103º 34' 18.01"
D24	AD	2018	4/6(15)-7(09)	47	2400	194	G24	N 43º 10' 55.20"	E 103º 07' 34.28"
D25	AD	2018	4/15(15)-16(10)	43	1300	316	G25	N 42º 56' 04.51"	E 102º 01' 39.43"
							G26	N 42º 56' 43.06"	E 101º 39' 04.13"
							G27	N 43º 06' 51.96"	E 101º 04' 28.67"
							G28	N 43º 18' 38.66"	E 101º 05' 31.79"
							G29	N 43º 26' 55.40"	E 101º 15' 28.02"
							G30	N 43º 56' 49.43"	E 101º 27' 19.13"
							G31	N 44º 02' 09.93"	E 101º 30' 26.83"
							G32	N 44º 25' 27.10"	E 101º 33' 49.81"
							G33	N 44º 41' 36.96"	E 101º 52' 59.77"
							G34	N 45º 05' 25.65"	E 102º 18' 03.50"

[1)]Dust sampling sites
AD: Andong, 36º 32' 34.76", 128º 47' 54.92"
DJ: Deokjeokdo, 37º 13' 59.47", 126º 08' 56.70"
SL: Seoul, 37º 36' 05.20", 127º 02' 49.02"

[2)] Transport time when PM_{10} concentration abruptly increased in the monitoring stations in Korea.

[3)] Distance from the eastern boundary of dust air parcel in outbreak area to Seoul, Korea.

[4)] Peak concentration of PM_{10} measured in the nearby monitoring stations operated by Korea Meteorological Administration.

783

784

785

786

787

788

789

790

Table 2. Mineral compositions of Asian dust (wt.%) determined by X-ray diffraction. Samples indicated by shades were collected during the same dust event.

Sample	Qtz[1)]	Pl	Kfs	ISCMs	Chl	Kln	Amp	Cal	Dol	Gp	Hl	Total clays	Pl/kf
D1	23.6	14.6	5.4	38.4	4.6	2.6	2.2	4.4	1.2	2.7	0.0	45.7	2.7
D2	24.2	13.9	6.8	41.6	3.1	1.4	2.7	3.1	2.0	1.3	0.0	46.2	2.1
D3	23.5	14.3	3.8	35.1	3.4	2.1	1.0	5.4	1.9	9.5	0.0	40.6	3.7
D4	18.0	12.2	4.7	35.1	5.9	3.1	2.4	4.4	2.4	11.7	0.0	44.0	2.6
D5	21.1	12.7	4.8	33.8	5.4	2.8	1.7	6.8	2.6	8.3	0.0	42.0	2.7
D6	18.2	10.9	4.8	34.1	5.7	3.1	2.1	8.7	2.6	9.7	0.0	42.9	2.3
D7	21.5	13.0	3.4	42.4	4.4	3.1	0.8	6.3	1.0	4.2	0.0	49.9	3.8
D8	18.7	12.6	6.0	45.9	4.5	2.1	2.7	3.8	1.1	2.5	0.0	52.5	2.1
D9	21.9	14.0	5.7	43.9	4.1	1.1	1.9	4.6	2.5	0.2	0.0	49.1	2.5
D10	28.7	17.5	5.6	33.5	3.5	2.3	0.9	6.3	0.8	0.8	0.0	39.3	3.1
D11	31.0	17.5	6.8	28.5	3.8	1.5	2.5	6.2	1.4	0.5	0.0	33.8	2.6
D12	19.1	12.2	7.1	33.7	2.2	1.8	2.1	1.2	2.4	18.3	0.0	37.8	1.7
D13	17.9	12.3	6.1	47.5	3.8	1.3	1.9	5.5	0.6	3.0	0.0	52.6	2.0
D14	18.3	13.4	5.3	47.9	1.8	1.9	1.0	0.5	0.4	9.4	0.0	51.6	2.5
D15	20.1	10.9	3.1	53.2	3.7	2.2	1.0	4.1	0.7	1.0	0.0	59.1	3.5
D16	19.7	11.3	3.7	49.5	3.7	2.7	1.0	3.4	0.6	4.3	0.0	56.0	3.0
D17	19.7	10.4	4.2	51.5	3.7	2.6	0.7	3.8	0.3	2.1	0.9	57.9	2.5
D18	19.0	10.5	4.3	51.9	3.1	1.7	1.3	2.8	0.5	5.1	0.0	56.7	2.4
D19	17.4	9.9	4.5	47.4	2.8	2.7	1.2	6.2	1.5	6.4	0.0	53.0	2.2
D20	17.1	10.5	5.7	39.2	4.1	2.0	2.4	9.2	1.9	8.0	0.0	45.3	1.9
D21	24.7	14.9	5.0	33.9	3.9	2.0	3.0	11.0	1.4	0.0	0.0	39.9	3.0
D22	19.9	10.5	4.0	41.3	4.4	2.0	3.8	8.5	2.4	3.3	0.0	47.7	2.7
D23	14.1	9.0	4.9	46.4	5.0	2.4	2.6	5.2	2.6	7.9	0.0	53.8	1.9
D24	19.0	10.6	6.1	46.4	4.8	1.3	3.0	3.8	1.3	3.6	0.0	52.5	1.8
D25	19.6	11.4	6.0	49.5	4.4	1.2	2.2	2.9	0.8	2.1	0.0	55.1	1.9
Average	20.6	12.4	5.1	42.1	4.0	2.1	1.9	5.1	1.5	5.0	0.0	48.2	2.5
St.dev.	3.7	2.2	1.1	7.1	1.0	0.6	0.8	2.5	0.8	4.4		6.9	0.6
Mineral compositions determined by SEM single particle analysis													
D13	19.0	10.9	3.8	53.8	2.4	1.1	0.7	7.0	0.8	0.5	0.0	57.3	2.9
D18	19.5	9.3	3.4	55.7	2.6	2.3	0.3	4.4	0.2	2.1	0.0	60.7	2.7
D19	16.9	7.9	2.6	50.2	4.9	2.3	0.6	9.4	2.5	2.7	0.0	57.4	3.1
D22	19.0	11.7	3.7	43.2	6.3	3.5	0.2	8.8	0.7	2.8	0.0	53.0	3.1
D24	21.0	9.7	4.4	50.9	4.0	1.5	0.8	4.8	0.8	2.0	0.0	56.4	2.2
SEM[2)]	19.1	9.9	3.6	50.8	4.1	2.1	0.5	6.9	1.0	2.0	0.0	56.9	2.8
XRD[3)]	18.6	10.8	5.0	46.9	3.8	1.8	2.2	5.4	1.3	4.3	0.0	52.5	2.2

[1)]Qtz, quartz; Pl, plagioclase; Kf, K-feldspar; ISCMs, illite-smectite series clay minerals; Chl, chlorite; Kln, kaolinite; Amp, amphibole; Cal, calcite; Dol, dolomite; Gp, gypsum; Hl, halite. [2) 3)]Average of five samples.

Table 3. Major element composition of Asian dust (unit in wt.%) on volatile-free basis. Samples indicated by shade were collected at different sites or serially during the dust event.

Sample	Si	Al	Fe	Mn	Mg	Ca	Na	K	Ti	P	Total	CIA*
D1	28.08	9.32	5.27	0.11	2.00	3.97	1.05	2.68	0.52	0.12	53.11	70.3
D2	28.48	9.17	5.19	0.12	1.83	3.54	1.20	2.75	0.53	0.16	52.97	68.1
D3	26.65	8.61	4.83	0.09	2.40	6.62	1.78	2.49	0.48	0.11	54.06	62.0
D4	25.67	9.17	5.28	0.11	2.65	6.59	1.57	2.71	0.48	0.12	54.34	64.7
D5	25.66	9.62	5.16	0.10	2.46	6.68	1.39	2.54	0.49	0.10	54.22	68.0
D6	24.98	9.08	5.17	0.11	2.68	7.93	1.47	2.77	0.47	0.12	54.75	65.2
D7	26.93	9.24	5.15	0.11	2.39	5.30	1.26	2.69	0.51	0.11	53.69	67.9
D8	27.24	9.69	5.54	0.11	2.20	3.87	1.17	2.80	0.54	0.19	53.35	69.5
D9	28.11	9.02	5.35	0.11	2.05	3.82	1.05	2.83	0.51	0.26	53.12	69.0
D10	27.72	8.38	4.95	0.11	2.15	5.34	1.91	2.42	0.51	0.12	53.61	60.5
D11	28.82	8.47	4.69	0.10	1.76	4.61	1.50	2.47	0.51	0.12	53.06	64.3
D12	25.19	9.00	5.56	0.15	1.99	7.27	1.89	3.03	0.53	0.19	54.78	60.6
D13	26.64	9.51	5.23	0.14	2.31	4.46	1.93	2.91	0.53	0.16	53.80	61.9
D14	27.59	9.37	5.35	0.13	1.89	3.80	1.42	3.16	0.55	0.16	53.42	65.1
D15	27.85	9.73	5.26	0.13	2.08	3.58	1.01	2.80	0.54	0.12	53.09	71.2
D16	27.59	9.60	5.38	0.13	2.10	3.91	1.09	2.80	0.53	0.13	53.26	70.0
D17	27.62	9.58	5.29	0.13	2.10	3.63	1.53	2.78	0.50	0.12	53.28	65.8
D18	28.09	9.44	5.17	0.12	2.03	3.61	1.21	2.79	0.52	0.11	53.09	68.5
D19	25.73	9.25	5.35	0.12	2.67	5.93	1.69	2.90	0.51	0.14	54.29	63.3
D20	25.22	8.89	5.29	0.12	2.53	7.45	1.71	2.86	0.51	0.15	54.71	62.3
D21	27.77	8.55	4.93	0.12	1.98	5.80	1.15	2.62	0.49	0.14	53.54	67.6
D22	25.96	9.36	5.76	0.12	2.47	5.98	1.11	2.66	0.50	0.17	54.09	69.7
D23	25.11	9.64	5.77	0.12	3.12	6.02	1.07	2.91	0.50	0.14	54.38	70.0
D24	27.75	9.62	5.31	0.11	2.11	3.68	1.09	2.90	0.50	0.12	53.19	69.8
D25	28.36	9.78	5.43	0.115	1.90	2.80	0.84	2.82	0.55	0.19	52.78	73.0
Average	26.99	9.24	5.27	0.12	2.23	5.05	1.36	2.76	0.51	0.14	53.68	66.7
St.dev.	1.21	0.41	0.25	0.01	0.33	1.48	0.32	0.17	0.02	0.04	0.62	3.5

*CIA: chemical index of alteration (Nesbitt and Young, 1982)

Table 4. Trace element composition of Asian dust (unit in ppm). Samples indicated by shade were collected at different sites or serially during the dust event.

Sample	S	Sc	V	Cr	Co	Ni	Cu	Zn	Ga	Rb	Sr	Y	Zr
D.L.*	10	1	5	20	1	1	1	1	1	1	2	0.5	1
D1	-	14	113	110	22	-	-	-	20	111	225	27.6	128
D2	-	13	113	110	33	-	-	-	18	107	217	26.9	139
D3	-	12	97	100	16	-	-	-	17	91	297	23.6	128
D4	2190	14	116	100	19	55	1280	500	19	101	326	24.9	119
D5	-	12	100	100	20	-	-	-	17	82	268	21.3	106
D6	-	13	111	190	17	-	-	-	18	99	315	23.2	108
D7	899	15	114	80	19	53	155	239	20	103	275	28.4	137
D8	-	13	101	100	19	-	-	-	19	101	208	25.7	111
D9	-	14	107	100	18	-	-	-	18	112	210	26.4	129
D10	1150	12	99	100	19	65	448	823	15	86	251	24.4	136
D11	440	12	96	100	17	54	218	415	18	103	237	26.7	148
D12	-	10	141	160	17	-	-	-	20	91	242	19.8	144
D13	-	12	102	90	18	-	-	-	18	91	224	22.4	106
D14	2500	12	113	100	18	68	1330	900	23	109	218	26.5	141
D15	420	15	118	190	20	53	166	157	21	115	218	29.7	125
D16	983	15	119	120	20	56	401	236	20	110	219	28.0	121
D17	581	14	104	80	19	51	219	184	20	108	203	26.6	108
D18	1190	13	108	90	19	53	2840	349	20	108	217	27.7	121
D19	-	13	97	110	18	34	1436	733	19	99	298	24.9	141
D20	-	12	95	100	16	-	-	-	17	88	290	21.8	144
D21	-	13	99	140	19	-	-	-	17	96	249	25.2	121
D22	-	14	123	110	21	-	-	-	19	100	272	26.6	116
D23	-	14	116	110	19	-	-	-	20	102	309	23.8	109
D24	-	14	105	100	19	-	-	-	19	109	210	25.7	109
D25	673	15	117	80	20	50	692	378	20	115	188	28.8	134
Average	1103	13	109	111	19	54	835	447	19	101	247	25.5	125

*Detection limit (ppm)

Table 4. *Continued.*

Sample	Nb	Sn	Sb	Cs	Ba	Hf	Ta	Tl	Pb	Th	U	La	Ce
D.L.*	0.2	1	0.2	0.1	2	0.1	0.01	0.05	3	0.05	0.01	0.05	0.05
D1	14.3	12	1.3	8.6	620	4.0	0.82	0.89	-	12.7	2.72	46.7	90.7
D2	12.4	61	0.3	8.6	622	3.7	0.72	0.72	-	12.2	2.73	41.3	81.0
D3	10.6	26	0.9	7.9	549	3.9	0.73	0.62	-	11.2	3.59	36.0	70.6
D4	11.6	29	4.5	9.1	571	3.4	0.69	0.86	250	11.9	3.78	35.5	71.7
D5	10.3	40	1.3	7.4	546	3.1	0.34	0.68	-	9.8	3.04	30.7	61.6
D6	11.0	39	2.6	8.4	589	3.0	0.69	0.60	-	11.3	3.64	33.1	66.5
D7	11.8	4	0.7	8.6	562	3.6	0.73	0.50	66	12.1	3.24	41.1	82.4
D8	12.1	7	< 0.2	8.3	519	3.8	0.65	0.56	-	11.2	2.84	37.3	75.7
D9	11.6	6	< 0.2	9.0	568	4.2	0.69	0.68	-	11.8	2.69	36.6	73.2
D10	13.0	5	0.2	6.5	589	3.9	0.59	0.44	199	10.9	2.50	44.1	85.5
D11	11.6	4	0.8	7.0	650	4.4	0.86	0.48	80	11.9	2.79	45.3	87.9
D12	10.8	96	4.0	7.7	788	4.0	0.67	1.17	-	10.1	2.85	34.4	63.5
D13	10.3	10	0.9	7.6	507	2.9	0.55	0.61	-	10.0	2.73	33.0	65.4
D14	11.5	41	2.9	8.9	699	4.2	0.77	0.87	264	12.6	3.07	38.6	77.1
D15	11.9	3	0.5	9.3	606	3.7	0.89	0.50	41	12.9	2.72	41.7	84.9
D16	12.5	3	< 0.2	9.0	612	3.6	0.77	0.47	78	12.2	2.71	40.5	82.7
D17	11.3	2	< 0.2	8.7	569	3.3	0.66	0.27	61	11.5	2.35	37.5	74.4
D18	12.7	3	< 0.2	8.8	599	3.5	0.79	0.53	104	11.7	2.59	38.0	77.8
D19	12.2	56	5.0	8.0	747	3.9	0.77	0.48	72.5	11.7	3.43	35.9	72.3
D20	10.4	39	1.9	6.7	778	4.1	0.58	0.52	-	10.9	3.28	32.6	64.4
D21	13.0	6	1.0	6.8	627	3.1	0.75	0.31	-	11.0	2.85	44.7	89.2
D22	12.1	7	2.4	8.2	625	3.5	0.84	0.55	-	12.2	3.30	43.8	84.4
D23	10.6	14	8.5	9.3	583	3.3	0.66	0.97	-	12.3	3.96	37.1	71.5
D24	12.4	3	1.1	8.9	597	3.2	0.79	0.53	-	11.5	2.39	38.6	77.5
D25	13.9	5	1.5	9.5	602	4.0	0.93	0.50	195	13.5	2.72	42.7	88.2
Average	11.8	21	1.7	8.3	613	3.7	0.72	0.61	116	11.6	3.0	38.7	76.8

*Detection limit (ppm)

Table 4. *Continued.*

Sample	Pr	Nd	Sm	Eu	Gd	Tb	Dy	Ho	Er	Tm	Yb	Lu	$(La/Yb)_N$[1)]	Eu/Eu*[1)]
D.L.*	0.01	0.05	0.01	0.005	0.01	0.01	0.01	0.01	0.01	0.005	0.01	0.002		
D1	9.83	36.5	6.55	1.50	5.24	0.77	4.73	0.93	2.61	0.388	2.51	0.374	12.5	0.78
D2	8.42	31.0	6.44	1.33	5.51	0.81	4.63	0.87	2.47	0.348	2.23	0.348	12.5	0.68
D3	7.39	27.5	5.55	1.07	4.52	0.69	4.34	0.84	2.27	0.332	2.26	0.330	10.7	0.65
D4	7.62	26.7	5.64	1.04	4.30	0.67	3.98	0.76	2.33	0.331	2.30	0.329	10.4	0.65
D5	6.51	25.2	4.78	1.02	4.01	0.65	3.79	0.72	1.99	0.287	1.84	0.261	11.2	0.71
D6	6.87	24.6	4.79	1.00	4.29	0.66	3.82	0.76	2.32	0.336	2.30	0.356	9.7	0.67
D7	9.19	32.9	6.09	1.34	5.11	0.75	4.64	0.91	2.65	0.411	2.64	0.390	10.5	0.73
D8	8.00	29.4	5.55	1.33	4.85	0.76	4.40	0.91	2.46	0.359	2.44	0.349	10.3	0.78
D9	8.13	30.8	6.27	1.30	4.92	0.78	4.51	0.85	2.50	0.391	2.29	0.343	10.8	0.72
D10	9.33	35.5	6.47	1.24	4.48	0.71	4.29	0.81	2.45	0.323	2.10	0.314	14.2	0.70
D11	9.74	36.7	6.50	1.30	5.14	0.78	4.61	0.85	2.44	0.355	2.36	0.345	12.9	0.69
D12	6.20	23.0	3.94	0.82	3.59	0.53	2.96	0.58	1.69	0.239	1.58	0.242	14.7	0.67
D13	7.04	25.8	5.00	1.16	4.09	0.61	3.88	0.71	2.08	0.305	1.97	0.327	11.3	0.78
D14	8.12	30.7	5.80	1.22	4.62	0.73	4.65	0.87	2.36	0.352	2.29	0.366	11.4	0.72
D15	9.12	34.1	6.62	1.33	5.65	0.86	4.93	0.97	2.77	0.415	2.84	0.432	9.9	0.66
D16	8.84	33.7	6.48	1.29	5.42	0.83	4.95	0.92	2.83	0.391	2.57	0.383	10.6	0.67
D17	8.22	29.9	6.10	1.23	5.13	0.80	4.54	0.88	2.54	0.356	2.20	0.342	11.5	0.67
D18	8.21	30.3	6.77	1.28	5.06	0.76	4.57	0.93	2.68	0.382	2.29	0.380	11.2	0.67
D19	7.51	28.9	5.63	1.18	4.49	0.69	4.03	0.77	2.22	0.324	2.24	0.326	10.8	0.72
D20	6.81	25.4	4.85	1.03	3.77	0.66	3.85	0.71	1.95	0.290	1.94	0.292	11.3	0.74
D21	9.91	34.9	5.54	1.33	4.43	0.69	4.36	0.77	2.23	0.301	2.02	0.324	14.9	0.82
D22	9.08	33.1	6.13	1.31	5.04	0.77	4.56	0.88	2.33	0.364	2.39	0.348	12.4	0.72
D23	7.37	26.5	5.36	1.12	4.07	0.67	4.10	0.83	2.37	0.355	2.10	0.302	11.9	0.73
D24	8.18	29.9	5.77	1.23	4.45	0.72	4.25	0.81	2.45	0.345	2.16	0.316	12.0	0.74
D25	9.22	34.7	7.39	1.30	5.50	0.87	5.12	1.01	2.75	0.399	2.54	0.384	11.3	0.62
Average	8.19	30.3	5.84	1.21	4.71	0.73	4.34	0.83	2.39	0.347	2.26	0.340	11.6	0.71

[1)] Values calculated from chondrite-normalized concentration. Chondrite values by Boynton (1984).

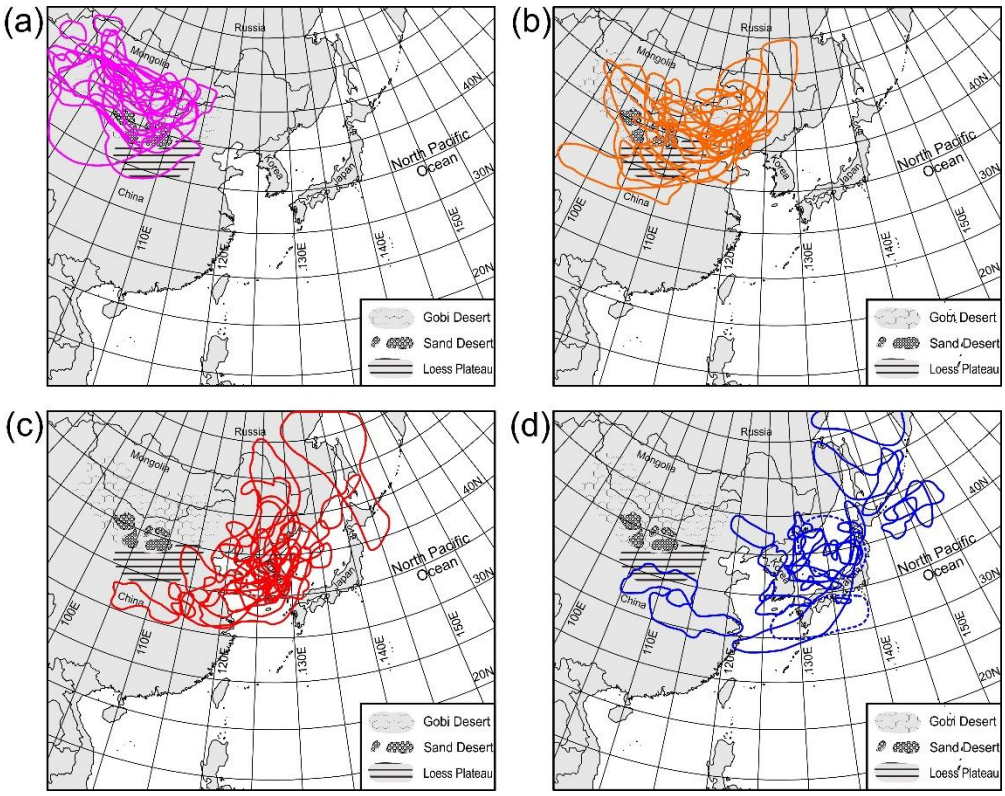

Figure 1. Dust storm outbreaks and migrations during 14 Asian dust events identified from the remote sensing images obtained from the Communication, Ocean, and Meteorological Satellite (COMS) (2011–2018) and the Multi-functional Transport Satellite-1R (MTSAT-1R) (2008–2010) satellites. The outbreak and migration path data for individual dust events are provided in Supplementary Fig. 1. (a) The maximum extent of the dust event during the storm outbreak. (b) Migration of dusty air toward the Korean Peninsula. (c) Dusty air crossing the Korean Peninsula. (d) Migration of dusty air toward the North Pacific Ocean.

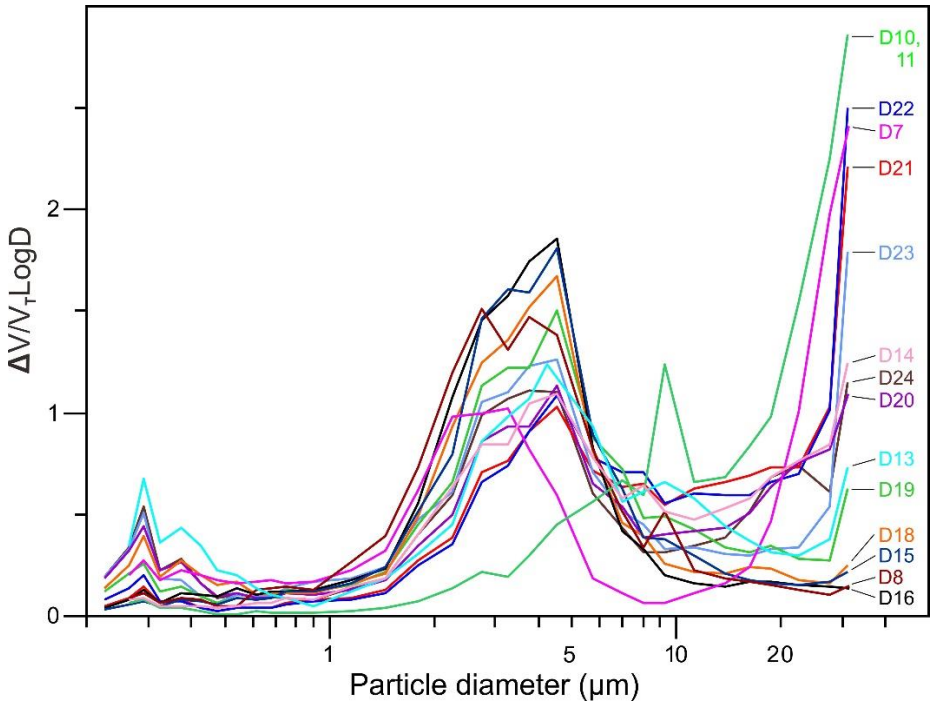

Figure 2. Volume-size distributions of aerosols during the Asian dust events, as measured by an optical particle counter located at the nearest Korea Meteorological Administration (KMA) monitoring stations. See Table 1 for the sampling site and time during the dust events.

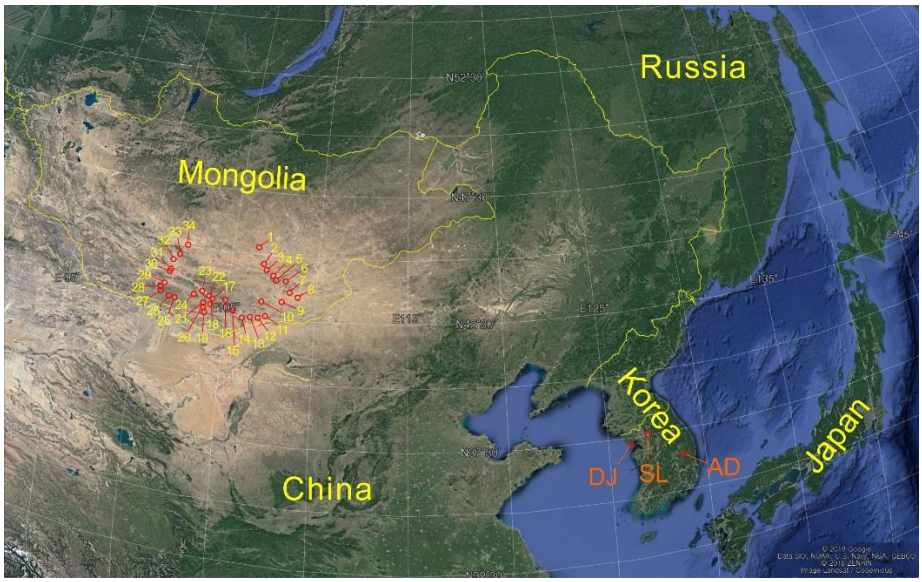

Figure 3. Three sites from which Asian dust samples were obtained in the Korean Peninsula, and the locations from which 34 soil samples were obtained in the Mongolian Gobi Desert. See Table 1 for the sampling site and time during the dust events. AD: Andong, DL: Deokjeok Island, SL: Seoul

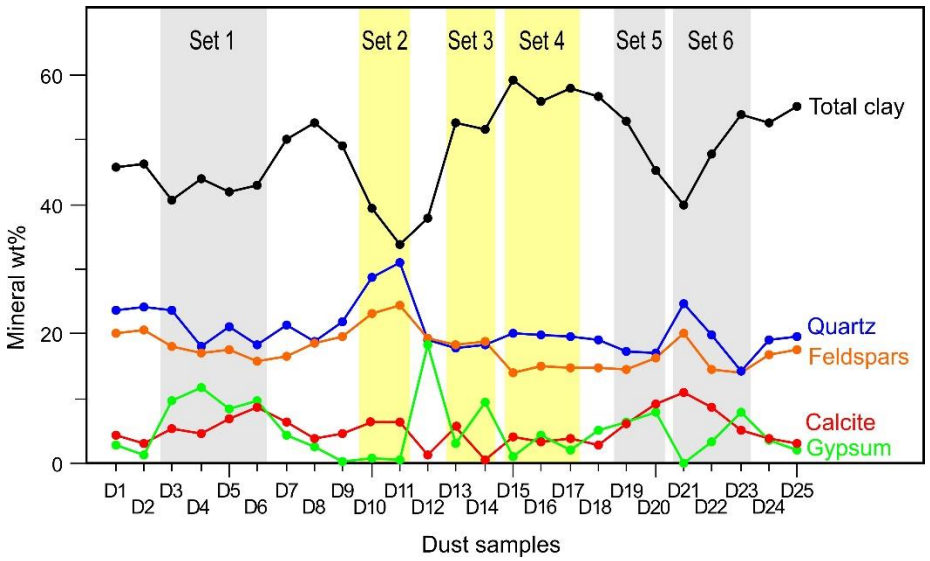

Figure 4. Time-series variation in the major-mineral contents of Asian dust. Sample collection dates are provided in Table 1. Dust samples set 1, 5, and 6 comprise serial samples collected during individual dust events. Dust sample sets 2–4 comprise samples collected at different sites during individual dust events.

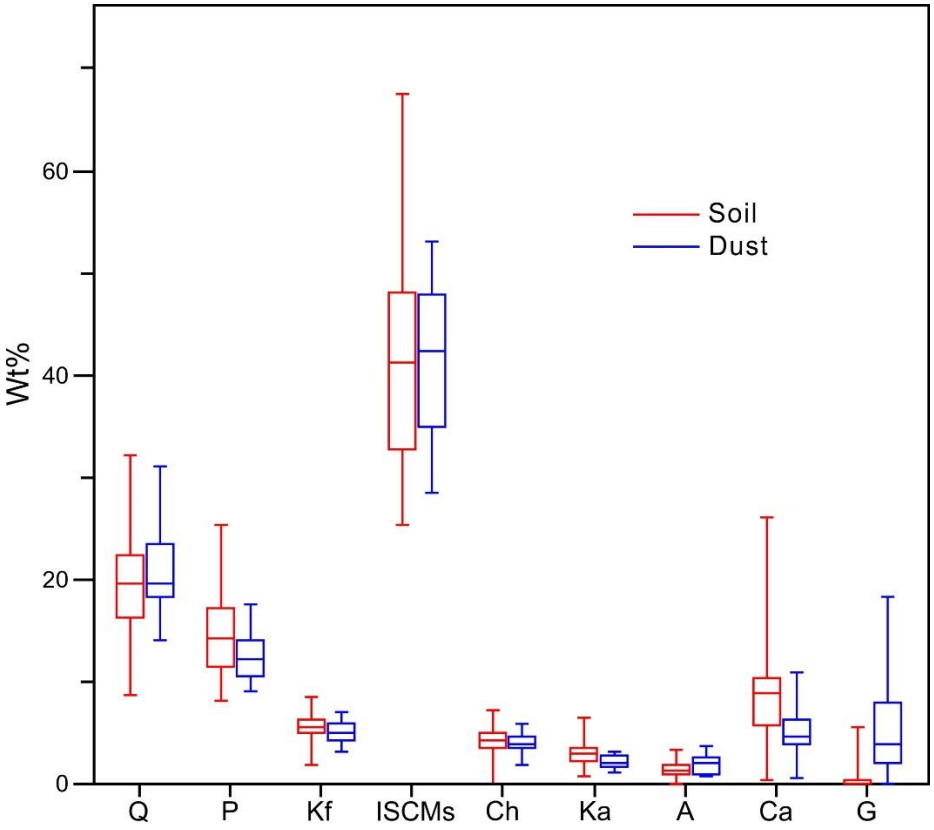

Figure 5. Box-whisker plot showing the mineral compositions of Asian dust and source soil samples. The top and bottom of the box define the third and first quartiles. The horizontal line in the center of the box is the second quartile, which is the median. The two ends of the vertical line crossing each box indicate minimum and maximum. Amp, amphibole; Cal, calcite; Chl, chlorite; Gp, gypsum; ISCMs, illite-smectite series clay minerals; Kln, kaolinite; Kf, K-feldspar; Pl, plagioclase; Qtz, quartz.

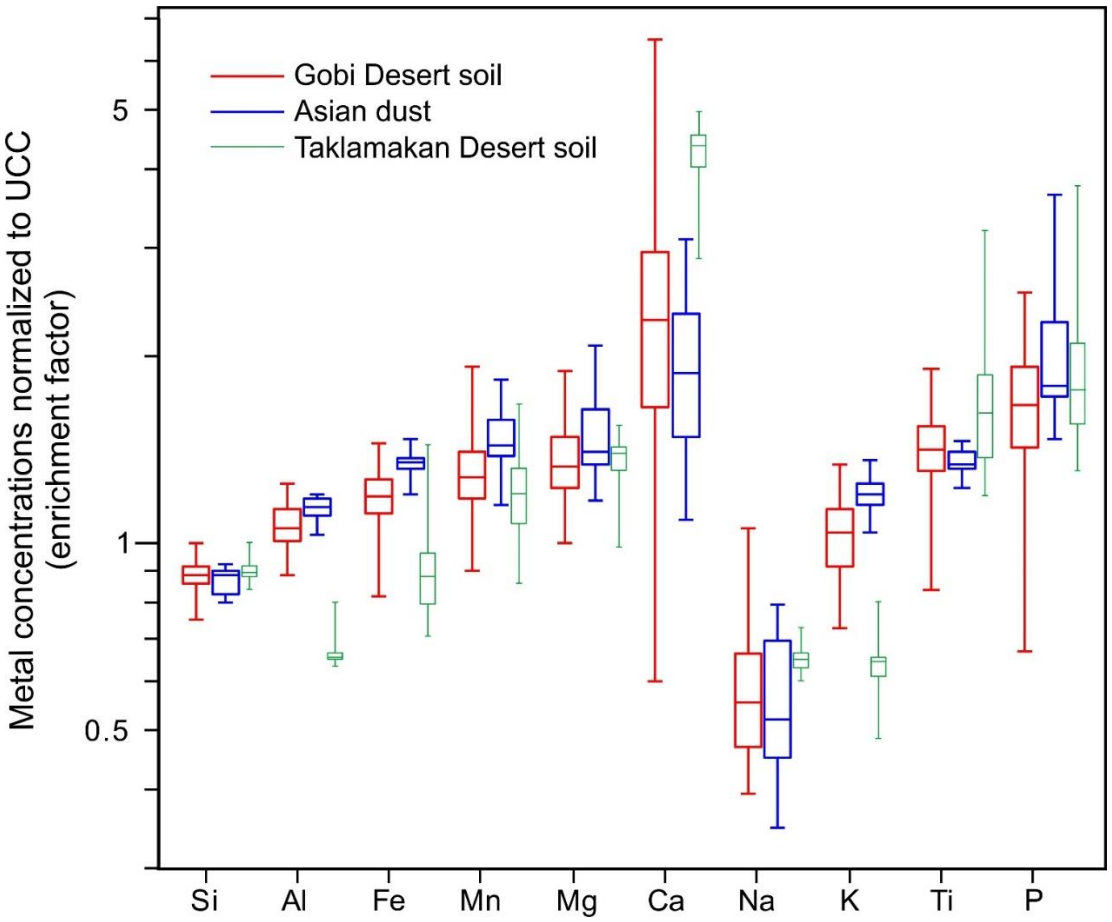

Figure 6. Box-whisker plot comparing the major element compositions between Asian dust and source soil samples, normalized to the average values of the upper continental crust (UCC) by Rudnick and Gao (2003). Data for Taklamakan Desert soils from Honda et al. (1998) (< 45 μm) and Jiang and Yang (2019) (< 63 μm).

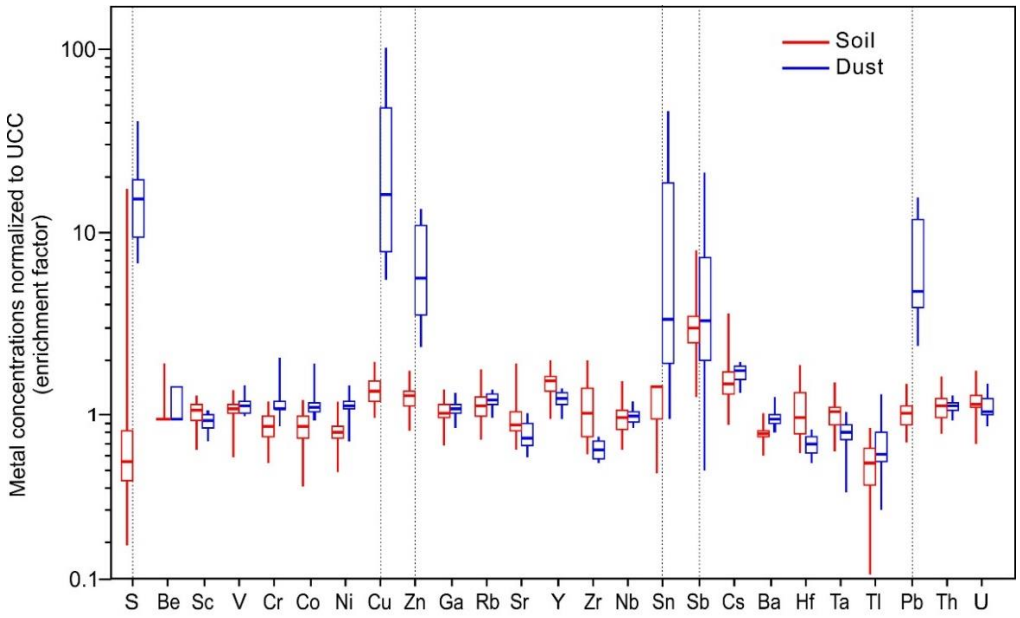

Fig. 7

Figure 7. Box-whisker plot comparing the trace element compositions between Asian dust and source soil samples, normalized to the average values of the UCC.

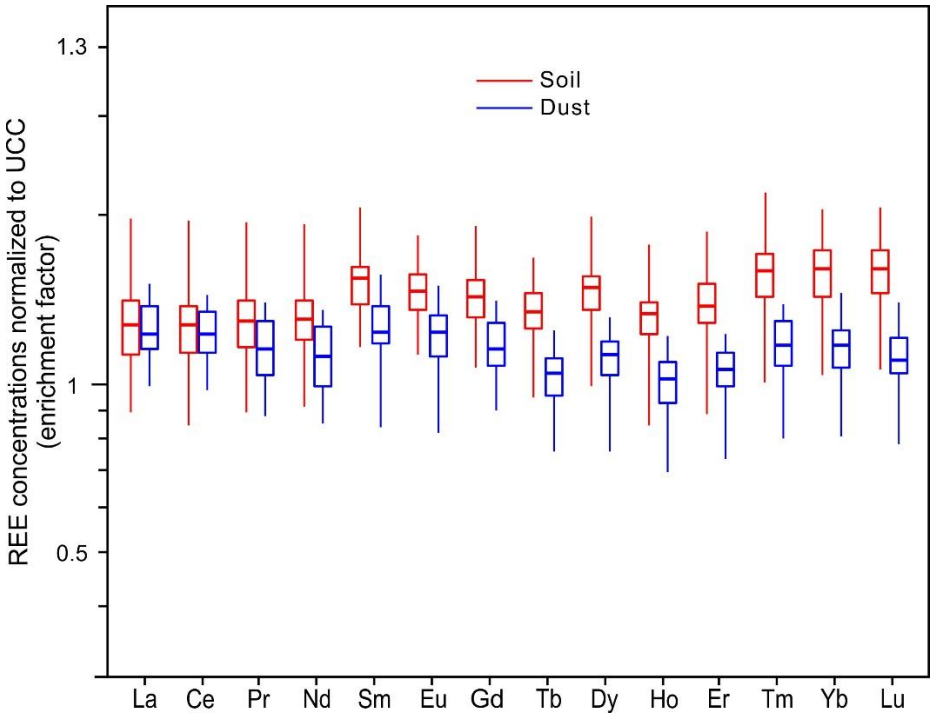

Figure 8. Box-whisker plot comparing the rare earth element compositions between Asian dust and source soil samples, normalized to the average values of the UCC.

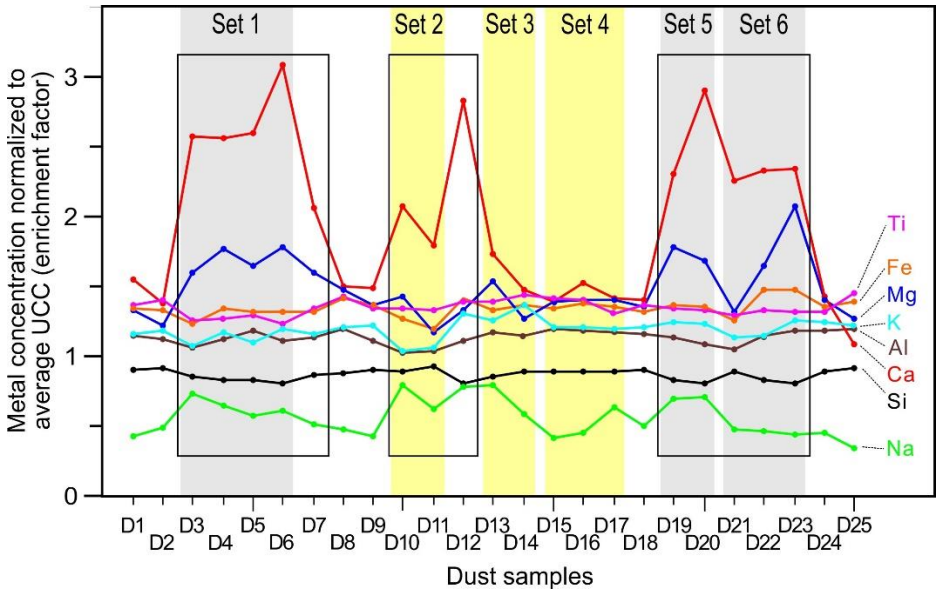

Figure 9. Time-series variation in major element compositions of Asian dust normalized to the average values of the UCC. Dusts in square boxes (D3–D7, D10–D12, D19–D23) were transported across the Chinese Loess Plateau and sandy deserts in northern China (Supplementary Figure S1). Sample collection dates are provided in Table 1. Dust sample sets 1, 5, and 6 are serial samples collected during individual dust events. Dust sample sets 2–4 are samples collected at different sites during individual dust events.

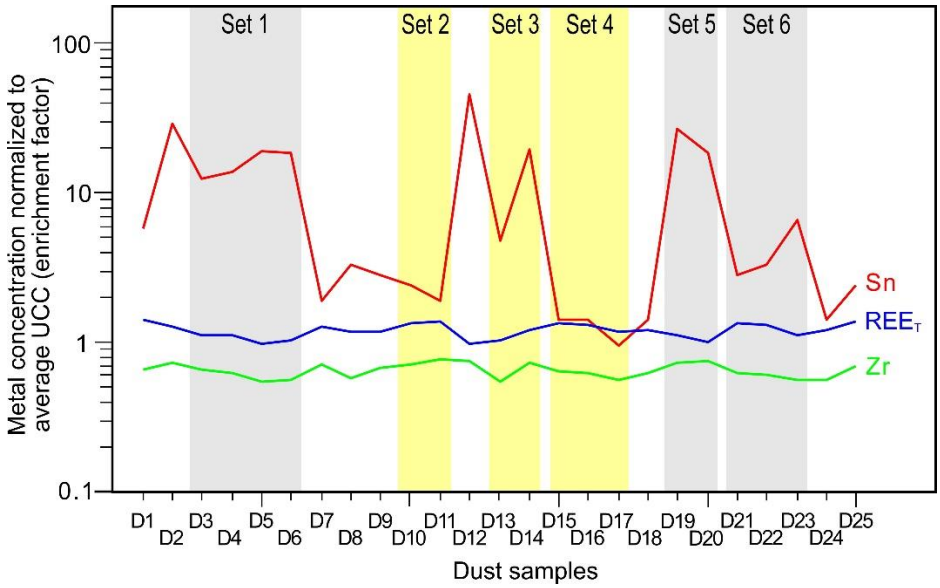

Figure 10. Time-series variation in trace element compositions of Asian dust normalized to the average values of the UCC.

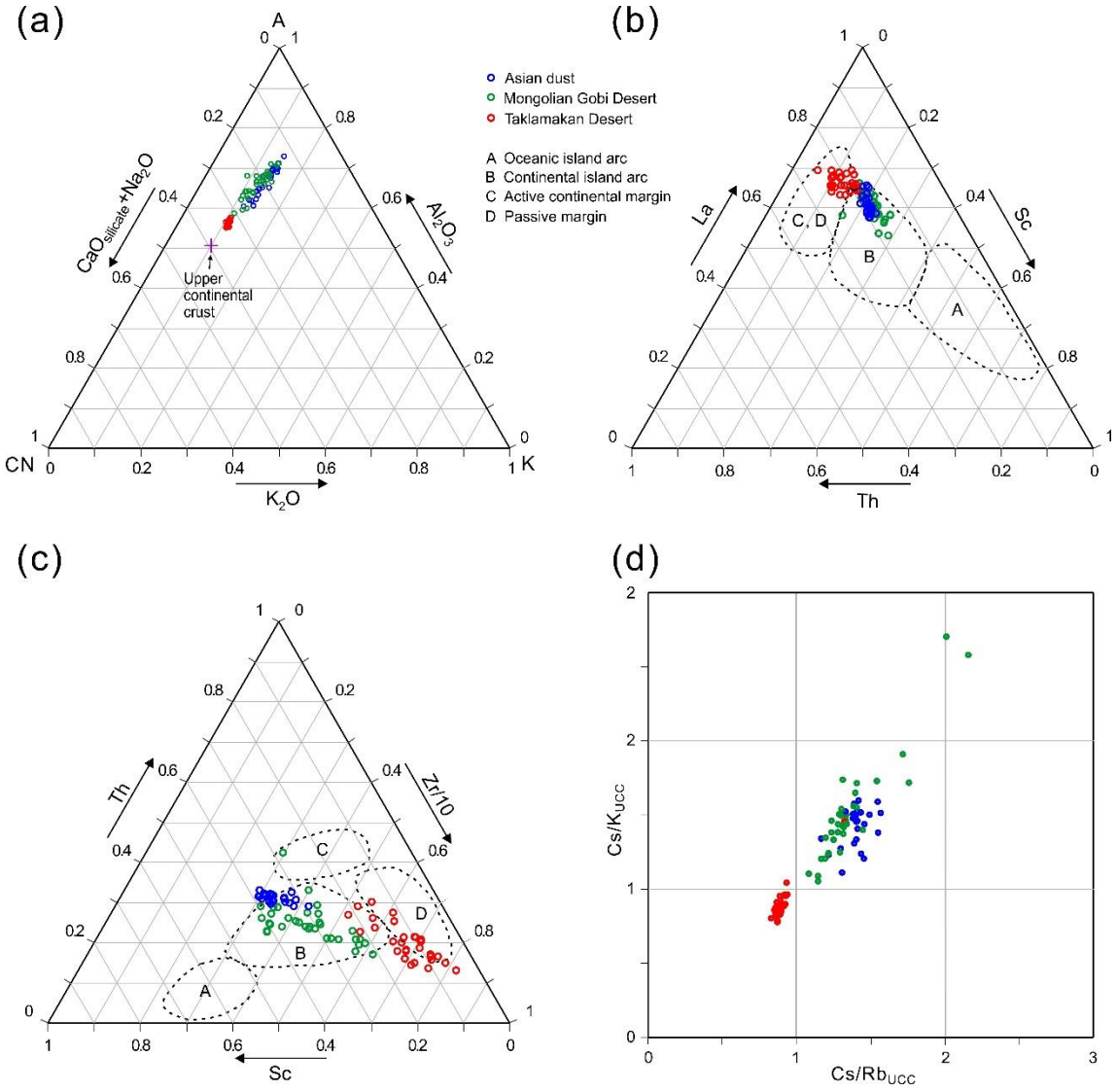

Figure 11. Plots of trace and major element compositions for discriminating the source of Asian dust. (a) A–CN–K diagram showing the molecular proportions of Al_2O_3, K_2O, and $CaO_{silicate}+Na_2O$. Value of Al_2O_3 is equivalent to CIA. $CaO_{silicate}$ was obtained by the correction of carbonate CaO (Honda and Shimizu, 1998). (b) La–Th–Sc plot. (c) Th–Sc–Zr/10 plot. (d) Cs/K_{UCC}–Cs/Rb_{UCC} plot. Data were normalized to UCC. Data of Asian dust and Mongolian Gobi Desert soils (< 20 μm) from this study. Trace element data for Taklamakan Desert soils from Jiang and Yang (2019) (< 63 μm). Major element data for Taklamakan Desert soils from Honda and Shimizu (1998) (< 45 μm) and Jiang and Yang (2019) (< 63 μm).